CMIP is a negative regulator of T cell signaling

Julie Oniszczuk, Kelhia Sendeyo, Cerina Chhuon, Berkan Savas, Etienne Cogné, Pauline Vachin, Carole Hénique, Ida Chiara Guerrera, Giuseppe Astarita, Vincent Frontera, et al.

CMIP is a negative regulator of T cell signaling

Julie Oniszczuk[1,2*], Kelhia Sendeyo[1,2*], Cerina Chhuon[3], Berkan Savas[1,2], Etienne Cogne[1,2], Pauline Vachin[1,2], Carole Henique[1,2], Ida Chiara Guerrera[3], Giuseppe Astarita[6], Vincent Frontera[1,2], Andre Pawlak[1,2], Vincent Audard[1,2,4,5], Dil Sahali[1,2,4,5†] and Mario Ollero[1,2]

1, Institut National de la Santé et de la Recherche Médicale (INSERM), UMRS 955, Equipe 21, Créteil, F-94010, France.

2, Université Paris Est, Faculté de Médecine, UMRS 955, Equipe 21, Créteil, F-94010, France.

3, Proteomic Platform Necker, PPN-3P5, Structure Fédérative de Recherche SFR Necker US24, 75015, Paris, France.

4, AP-HP, Groupe Henri-Mondor Albert-Chenevier, Service de Néphrologie, Créteil, F-94010 France.

5, Institut francilien de recherche en néphrologie et transplantation.

6, Department of Biochemistry and Molecular &Cellular Biology, Georgetown University, Washington, DC, USA.

*****These authors contributed equally to this work.

†Address correspondence to Dil Sahali, INSERM U 955. Phone : 33149812537 ; Fax : 33149812539 ; email : dil.sahali@inserm.fr

Running title: CMIP inhibits T cell signaling

Abstract

Upon interaction with cognate antigen, T cells integrate different extra and intracellular signals, involving basal and induced protein–protein interactions as well as binding of proteins to lipids, which can lead to either cell activation or inhibition. Here we show that selective T-cell expression of CMIP, a new adaptor protein, by targeted transgenesis drives T cells toward a naïve phenotype. We found that CMIP inhibits activation of Src kinases Fyn and Lck after CD3/CD28 costimulation, and their subsequent localization to LR. Video microscopy analysis shows that CMIP blocks the recruitment of LAT and the lipid raft marker cholera toxin B at the site of TCR engagement. Proteomic analysis identified several protein clusters differentially modulated by CMIP and notably Cofilin-1, which is inactivated in CMIP-expressing T-cells. Moreover, transgenic T cells exhibited a downregulation of GM3 synthase, a key enzyme involved in the biosynthesis of gangliosides. These results suggest that CMIP negatively impacts proximal signaling and cytoskeletal rearrangement and defines a new mechanism of negative regulation of T-cells, which could be considered as a potential therapeutic target.

Introduction

T cells play a central role in adaptive immunity through a close interplay with humoral and cellular sensors of innate immunity (1). T-cell activation is initiated by ligation of the TCR by an appropriate peptide bound to a major histocompatibility complex (MHC) molecule, which triggers rapid Src kinases-mediated phosphorylation of the immunoreceptor tyrosine-based activation motif (ITAM), a conserved domain of signal transducing chains of the TCR complex (2). Phosphorylated ITAMs serve as binding sites for ZAP-70 kinase, which is activated by phosphorylation by the Src kinase Lck resulting in stability of the ITAM-ZAP 70 interaction. The clustering of active TCR and the recruitment of Src kinases, Lck and Fyn in T cells, and ZAP-70 occurs in lipid rafts (LR), which are plasma membrane microdomains enriched in cholesterol and glycosphingolipids and serve as signaling platforms (3). Activation of ZAP-70 induces phosphorylation at multiple tyrosine residues of the transmembrane adapter molecule LAT (linker for activation of T-cells) and leukocyte phosphoprotein of 76 kDa (SLP-76) contributing to generate through protein-protein or protein-lipid interactions a signaling multicomplex within LR. Activation of costimulatory molecules such as CD28 promotes the recruitment of kinases and adaptor proteins within LR, which induce cytoskeletal reorganization leading to formation of immunological synapse. Immobilization of signaling molecules by cytoskeletal actin filaments and scaffold proteins may facilitate more efficient signal transmission from rafts to downstream signaling cascades, ultimately resulting in activation of transcription factors such as NF-kB, NFAT, and AP-1 (4).

CMIP (C-Maf-inducing protein) was Initially identified in T cells of patients with minimal change nephrotic syndrome (MCNS), a renal disease of unknown immune origin (5). The predicted structure of the 86-kDa natural isoform of CMIP includes an N-terminal region containing a pleckstrin homology domain (PH), a middle region characterized by the presence

of several interacting docking sites, including a 14-3-3 module, a PKC domain, three potential ERK domains and an SH3 domain similar to the p85 regulatory subunit of phosphatidylinositol 3-kinase (PI3K), as well as a C-terminal region containing a leucin-rich repeat (LRR) domain.

CMIP expression has been further found overinduced in podocytes during INS relapse and in membranous nephropathy, another immune–mediated glomerular disease (6, 7). Recent studies show that CMIP is also induced in some T cell subsets in patients with active systemic lupus erythematosus (8), as well as with INS-like disease associated with cancers (9, 10). Increased CMIP abundance in these various pathological conditions may reflect different mechanisms of induction, possibly cell specific. In fact, CMIP moves from cytoplasm to plasma membrane through its PH domain, or to the nuclear compartment via its nuclear localization site, this shuttling implying interactions with different partners. For instance, several partners have been identified by yeast-two-hybrid system and confirmed by immunoprecipitation including, among others, Src kinase Fyn, P85 subunit of PI3 kinase, RelA (p65 subunit of NF-kB), filamin A, DIP-1 (death-associated protein kinase (DAPK)-interacting protein 1) (11-13). By interacting with RelA, CMIP prevents its nuclear translocation and inhibits NF-kB activation (11, 14). In podocytes, CMIP promotes apoptosis by inducing caspase-3 activity, an upregulation of the pro-apoptotic protein Bax and a decrease of the antiapoptotic protein Bcl-2 (15). However, CMIP is scarcely detectable at both the transcript and protein levels in adult tissues in physiological conditions, at least partly due to its transcriptional repression, notably by NF-kB and WT1, two master transcription factors (16, 17).

The raise in CMIP transcript levels in lymphocytes from patients constitutes one of the hallmarks of MCNS relapses (6), strongly suggesting a potential involvement in disease pathogenesis and in the regulation of immune response, but its precise role is currently

unknown. Given that sequence analysis of CMIP coding regions shows strong identity (99%) between human, mice and rat, we have generated transgenic mice overexpressing CMIP selectively in mature lymphocytes. In the present study, we aimed to understand the role of CMIP in T-cell signaling by thoroughly observing the impact of its overexpression on T-cell response.

Results

Expression of CMIP in human T-cells

We first analyzed the expression of CMIP at the mRNA and protein levels in patients with MCNS relapse and remission as well as in control healthy subjects. The expression of the transcript was measured by real-time quantitative PCR (RT-qPCR), each patient being analyzed in relapse and in steroid-free remission (n=10). The transcript level in patients was quantified as -fold induction relatively to control subjects. We found relapses associated with a significant increase of CMIP abundance (Figure 1a). Western-blots from PBMC lysates showed a slight band recognized by polyclonal CMIP antibody at the expected size in patients with relapse (Figure 1b) but not or scarcely detected in remission. Immunofluorescence analysis indicates that CMIP was expressed selectively in a subset of T cells (Figure 1c), but the unavailability of CMIP-specific monoclonal antibodies still precludes accurate characterization of this subset by flow cytometry.

Generation of CMIP transgenic mice

To analyze the functional consequences of CMIP overexpression *in vivo*, we used a targeting system in which a construct containing a single copy of the human CMIP coding sequence downstream of the Lck distal promoter was inserted into the X-linked hypoxanthine phosphoribosyltransferase (Hprt) locus by homologous recombination (Figure 2a). It has been established that Lck distal promoter drives transgene expression in peripheral T-cells (18). We obtained six founders, which were crossed with WT (WT) BALB /c mice and backcrossed repeatedly to obtain a homogeneous BALB /c genetic background. Because the transgene is expressed in the X chromosome, all mice analyzed within the current study were hemizygous males from F10 to F18 generation and confirmed by tail genotyping (Figure 2b). Transgene expression was demonstrated at the

transcriptional level in splenic T cells (Figure 2c). Although the endogenous CMIP transcript was detected in WT (control littermates) splenic T-cells, immunofluorescence labeling using two different polyclonal antibodies detected a significant signal in transgenic mice, but scarcely in WT (Figure 2d). Examination of thymus, node and spleen during the follow-up showed that the basal phenotype of transgenic mice was substantially normal and no lymphoproliferative syndrome was observed until one year of age.

CMIP transgenic mice exhibit a "naïve" T-cell phenotype

To assess the influence of CMIP expression on T-cell compartments, we determined by FACS analysis the frequency of the main peripheral T-cell subsets. Splenocytes from 12-week old mice were purified and stained with CD4, CD8, CD44 and CD62L antibodies. Although the number of CD3 T cells and the percentage of either $CD4^+$ or $CD8^+$ T cells was comparable between WT and transgenic mice (n= 5 mice for each group) (Figure 3a and b), the frequency of naive $CD4^+$T cells ($CD4^+CD44^{low}CD62L^{high}$) and naïve $CD8^+$T cells ($CD8^+CD44^{low}CD62L^{high}$) were significantly increased in Tg mice, whereas the frequency of memory and effector T cells ($CD44^{high}CD62L^{high}$ and $CD44^{high}CD62L^{low}$, respectively) was decreased in both Tg $CD4^+$ and $CD8^+$ T cells (Figure 3c and d). We next analyzed T-cell proliferative ability following CD3/CD28 stimulation. T cells were cultured *ex vivo* in quiescent conditions (six hours in the presence of 2% FCS), and then incubated in 10% FCS complete medium in the presence of anti-CD3/CD28 antibodies (1 µg/ml each). After staining with CFSE at day 0, T cells were allowed to proliferate for 5 days, then analyzed by flow cytometry. As attested by CFSE dilution, the percentage of dividing cells was lower in transgenic T cells as compared with WT, while addition of IL-2 in the culture medium restored the proliferative capacity of transgenic T cells to control levels (Figure 3e and Figure S1).

Transgenic T cells display an impaired response to CD3-CD28 stimulation

We sought to determine the effects of *in vivo* overexpression of CMIP on T-cell activation and polarization. We first studied the CMIP transgene expression in T cells isolated by negative immunoselection, under resting and stimulating conditions. T cells were starved in RPMI medium containing 2% FCS for six hours at 37°C, then activated with anti-CD3/CD28 (1µg/ml each). The abundance of the endogenous CMIP transcript quantified by RT-qPCR, rapidly fell upon CD3/CD28 stimulation and the endogenous protein was scarcely detected by Western-blot (Figure 4a and b). On the other hand, the CMIP transgene expression, driven by the Lck distal promoter, was significantly increased at the mRNA and protein levels at early stages and reached a peak one hour after activation (Figure 4a and b). In physiological conditions, T-cell activation is associated with a strong induction of NF-kB activity. Previous reports have shown that NF-kB is a repressor of CMIP transcriptional activation (11, 14), which may account for the downregulation of endogenous Cmip in WT mice.

We next analyzed whether expression of CMIP transgene was associated with a particular pattern of cytokine production in T cells isolated by negative immunoselection. Because transgene abundance started a decline from 2h post-activation, we analyzed cytokine expression during 16 hours following CD3/CD28 activation, by RT-qPCR, except for IL2 of which the transcription started earlier after T cell stimulation. As compared with T cells from WT, transgenic T cells exhibited a significant lower amount of IL-2, IL-4 and IFNγ, whereas IL-10 was increased (Figure 4c). To assess whether cytokine production was affected by signals bypassing TCR stimulation, T cells were isolated by negative immnoselection and challenged with phorbol myristate ester (PMA, 50 ng/ml) and ionomycin (0.5 µg/ml). While lower IL-2 production was found in Tg T cells stimulated by CD3/CD28, no significant difference was noticeable following PMA/ionomycin activation between WT and Tg T cell

(Figure S2). By contrast, higher levels of IL-4 and IFNγ transcripts were detected in WT T cells after 4h PMA/ionomycin activation, although the differences were less pronounced than with TCR signals. Noteworthy, the increased abundance of IL-10 mRNA level in Tg T cells after CD3/CD28 stimulation was not found with PMA/ionomycin activation, which suggests that proximal signals rising from Tg T cells are required for IL-10 synthesis. Altogether, these results suggest that increased Cmip abundance is mainly associated with an inhibition of T-cell activation and differentiation into effector T cells.

CMIP expression is associated with inactivation of Src kinases

In physiological situations, T-cell activation results in a series of phosphorylation cascades that ultimately result in cellular proliferation, differentiation and cytokine production. The lower reactivity of transgenic T cells in response to CD3-CD28 stimulation led us to investigate whether they display a phosphorylation defect in some components playing a key role in early signaling. T cells were synchronized (six hours in the presence of 2% FCS), then stimulated with anti-CD3/CD28 antibodies, total protein lysates were collected at one hour post-activation, and analyzed by Western blotting using the anti-phosphotyrosine monoclonal antibody 4G10. Wild-type T cells exhibited major phosphorylation within a region spanning 60-70 kDa, which was barely detected in Tg T cells (Figure 5a). This region includes, among others, the members of the Src kinase family, which are involved in the early steps of T-cell activation (19). Src kinase family comprises nine members of which, Lck and Fyn are the most abundant in T cells and play a crucial role in immune response (20). Therefore, we tested the reactivity of protein lysates with an anti-Src antibody that recognizes the phosphotyrosine (pY) site at the 418 residue, specific of active Src kinases. A decrease of pY^{418}Src in transgenic T-cells was clearly observed, culminating 15 min after activation, which coincides with the highest levels in WT T cells (Figure 5b). The early events of T-cell activation involve the clustering of T-

cell receptor and costimulator molecules, as well as the recruitment of Src kinases Fyn and Lck into LR (3). Lck phosphorylates ITAM motifs at intracellular CD3 domains and induces ZAP70 recruitment (21). We evaluated the levels of pY^{505}Lck and pY^{528}Fyn, specific of the inactive forms, after T-cell stimulation. The abundance of pY^{505}Lck and pY^{528}Fyn was increased in transgenic T cells at baseline and persisted after CD3/CD28 stimulation when compared with WT T cells (Figure 5c and d). We examined the phosphorylation levels of ZAP70 and observed a remarkable increase of its active form (pY^{319}Zap 70) in WT T cells upon stimulation, but not in transgenic T cells (Figure 5e). Interestingly, immunofluorescence analysis showed that pY^{418}Src was confined to a clustered compartment within the thin layer of sub-plasma membrane at 30 and 60 min post-activation in WT T cells, this formation was not detected in Tg T cells (Figure 5f). Overall, these results suggest that CMIP inhibits the first steps of T cell activation. This possibility was further assessed in Cmip-deficient T cells, in a new mouse model of a selective and doxycycline-inducible *CMIP* ablation in T cells (CD2-rtTA/TetOn-Cre/$CMIP^{loxP/loxP}$). Naïve CD4 T cells were purified from KO and control littermates (without doxycycline treatment) and stimulated by anti-CD3/anti-CD28 (1 µg/ml each) for 15 and 30 min (Figure S3). As compared with T cells from controls, the level of inactive forms of Src kinases Fyn and Lck was lower in Cmip-deficient T cells, whereas the abundance of active pY^{418} Src kinases and pY^{319}Zap70 was increased (Figure S3, a-d). Genotyping and Western blotting confirm that Cmip was expressed in control littermates and deleted in KO mice (Figure S3e).

Transgenic T cells show accumulation of inactive Fyn and Lck in LR

We investigated whether the clustering of LR is compromised as a result of impaired Src kinase activation in transgenic T cells. We purified LR by a detergent-free OptiPrep method, in resting conditions and 30 min following activation by anti-CD3/CD28

antibodies (1 µg/ml each). We tested the distribution of flotillin-1 and cholesterol by Western blotting and thin layer chromatography (TLC) respectively and found them enriched in LR fractions. The observed difference in flotillin-1 and cholesterol signal between WT and Tg LR is due to a difference in input amounts (Figure 6a). Both total forms of Fyn and Lck were found mostly localized to LR with similar proportions, except in transgenic T cells, where total Lck was reduced in LR after 30 min activation. In resting conditions, the relative abundance of pY^{528}Fyn (inactive form) in LR was twice higher in transgenic T-cells as compared to WT (Figure 6a and b). In activated T-cells, the relative abundance of pY^{528}Fyn was dramatically increased in transgenic T cells, whereas it remained at low levels in WT. Although we found no difference in its abundance in resting conditions, pY^{505}Lck was significantly increased in LR in activated transgenic T cells as compared to WT (Figure 6a and c). These results suggest that the lower reactivity of transgenic T cells may result from an inactivation of Src kinases in LR linked to CMIP-mediated inhibition of proximal signaling.

Transgenic T cells fail to polarize during CD3/CD28 costimulation

T-cell polarization after CD3/CD28 stimulation involves the migration and aggregation of lipid raft microdomains at the site of immunological synapse formation (22).

We evaluated whether the distribution of LR in transgenic T cells was affected using the lipid raft marker cholera toxin B (CTB), which binds preferentially the ganglioside M1 (GM1) glycosphingolipid. We performed double fluorescence labeling with anti-Src antibody and CTB. WT T cells exhibited a polarized colocalization of both markers after 30 min post-activation (Figure 7a). However, we did not detect any polarization in transgenic T cells, suggesting that CMIP interferes with LR migration. Then, we analyzed the linker for activation of T-cells (LAT), an adaptor protein that is recruited at the plasma

membrane and segregates into LR upon engagement of T-cell receptor and costimulatory signaling. The membrane localization and distribution of LAT and CTB (coupled with Alexa Fluor 555) were examined by fluorescence staining 30 min after T-cell activation by anti-CD3/CD28 (1µg/ml each). While LAT and CTB were clustered in plasma membrane microdomains in WT T cells, they were spread along the plasma membrane in transgenic T cells (Figure 7b). We next monitored of LR dynamics following anti-CD3/CD28 costimulation. T cells from transgenic and WT mice were isolated by negative immunoselection and stained with AF555-CTB, then incubated in the presence of anti-CD3-coated beads and soluble anti-CD28 (1µg/ml). The time-dependent distribution of fluorescence was evaluated by videomicroscopy. We observed that CTB moved from the periphery and formed a cluster at the contact point between T-cell and CD3-beads (Figure 8c and movie S1). Conversely, CTB did not move towards CD3-beads in transgenic T cells, suggesting that they were unable to reorganize GM1 positive microdomains. Collectively, these results suggest that CMIP prevents the LR clustering required for the formation of immunological synapse and effective T-cell activation.

CMIP alters the glyco/ganglio-sphingolipid metabolism

To examine whether CMIP overexpression modifies the dynamics and the lipid composition of cell membranes, we used an independent cell line -immortalized mouse podocytes stably transfected with the CMIP coding sequence- that we had optimized for untargeted global lipidomics analysis. Principal component analysis (PCA) of our lipidomic data showed a clear clustering of our samples into two groups, discriminating CMIP-transfected from empty vector-transfected control cells (EV). Figure 8a shows a PCA in which both positive and negative ions are combined. The lipids that contributed most to the variance between groups were isolated using ANOVA $p<0.001$ and -fold change > 5. Pathway topology analysis searching among KEGG pathways using Metabolomics Pathway Analysis (MetPA) showed

that CMIP expression had a strong impact on sphingolipid metabolism (Figure 8b). Additionally, an independent over-representation analysis across multiple pathways sources using IMPaLa confirmed that the most significant alteration affected the glyco/ganglio-sphingolipid metabolism (Data file S1). Consistently, the levels of GM3 and GM2 species showed a significant decrease, whereas the levels of GM1 species increased in CMIP-expressing compared to control cells (Figure 8c). To understand the mechanism leading to these modifications in the ganglioside profile, we evaluated by western blot the expression level of GM3 synthase, a key enzyme in the biosynthesis of the ganglio-series, responsible for the conversion of LacCer into GM3. We observed a decreased expression of GM3 synthase, in Tg as compared to Wt cells, especially at 30 and 60 min post activation (Figure 8d). This suggests that a decrease in GM3 synthase expression could contributes, at least in part, to the downregulation of GM3 and GM2 observed in cells overexpressing CMIP.

Proteomic analysis of T-cells isolated from WT and transgenic mice

To further evaluate the impact of CMIP expression on T-cell signaling, we performed differential proteomic analysis of T cells from 12-week old transgenic and WT mice (twelfth generation, n=3 each). T cells were purified by negative immunoselection, then activated by anti-CD3/CD28 antibodies (1µg/ml each). At 0 and 60 min post-stimulation (corresponding to higher expression of the transgene), total proteins were extracted, trypsin digested, and peptides quantified on three parallel technical replicates per sample. The expression levels of the 2660 identified proteins were compared in the four conditions (Data file S2). As a result, 46 proteins were found differentially expressed between transgenic and WT as a function of T-cell activation (two-way ANOVA interaction, $p<0.05$) (Data file S3). Hierarchical clustering displayed four major clusters, grouping those proteins varying comparatively in the different experimental conditions (Figure 9a and Table 1). In basal conditions, a cluster of 9 proteins (cluster 1) was found highly

expressed in WT T cells while it was strongly downregulated in transgenic T cells. This cluster includes two proteins involved in lipid remodeling, namely the HRAS-like suppressor 3 (Pla2g16) and ethanolamine phosphate cytidylyltransferase (Pcyt2). In activated T-cells, a cluster of 13 proteins (cluster 2) that were found depleted in WT but increased or unchanged in transgenic mice. This cluster includes proteins involved in the organization of actin cytoskeleton, like cofilin-1 (Cfl1), and in nucleotide metabolism, like creatine kinase B-type (Ckb), nicotinamide phosphoribosyltransferase (Nampt) and guanylate kinase (Guk1). Cluster 3 encompassed 10 proteins that were significantly downregulated in WT relatively to transgenic T cells in basal conditions. This cluster includes two proteins involved in lipid uptake and metabolism, namely cell cycle control protein 50A (Tmeme30a) and monoacylglycerol lipase (Abhd6). Most remarkably, a fourth cluster (cluster 4) comprised 14 proteins undergoing a dramatic increase after stimulation in WT, but being depleted in transgenic T cells under the same conditions. Representative members of this cluster were, most notably, the inhibitor of nuclear factor kappa-B kinase subunit epsilon (Ikbke), casein kinase II subunit alpha (Csnk2a2), the cPLA2 inhibitor annexin-1 (Anxa1), as well as the lipid remodeling factor lysophosphatidic acid phosphatase 6 (Acp6). These results, along with other data obtained from the transgenic mouse model, point at a defect in T-cell activation associated with CMIP expression. Based on these findings, we further analyzed by Western blotting the expression of Cofilin-1, a major actor of dynamic rearrangement of actin cytoskeleton (23) whose activity has been recently reported to be negatively regulated by CMIP in podocytes (24). We found that phosphorylation of Cofilin-1, corresponding to its inactive form, was dramatically increased in transgenic T cells at 60 min post-stimulation as compared to WT T cells (Figure 9b). Likewise, Cofilin-1 was found hyperphosphorylated in HEK cells overexpressing CMIP compared to cells transfected with a control vector (data not shown),

suggesting a functional connection between CMIP overexpression and Cofilin-1 inactivation.

Discussion

Little is known about the role of CMIP *in vivo* and the functional consequences of its overexpression in T cells. This led us to generate a transgenic mouse model in which CMIP is selectively induced in peripheral T-cells. We show for the first time that CMIP: (i) interferes with the early events of T-cell signaling by inhibiting the activation of Src kinases (Fyn and Lck) and Zap-70 and their localization to LR; (ii) inhibits LR clustering, which is required for immunological synapse formation; and (iii) transgenic T cells exhibit a lower proliferative capacity and are less prone to producing cytokines after stimulation. In addition, transgenic mice display a higher percentage of T cells with a naïve T-cell phenotype, as well as a lower reactivity to CD3/CD28 stimulation, as reflected by a decrease in IL-2 production. The inability to produce sufficient amounts of IL-2 may explain why transgenic T cells fail to proliferate and to differentiate like WT T cells. However, the addition of recombinant IL-2 to the culture medium restores their proliferative capacity. These results are consistent with previous data obtained from a randomized multicenter clinical trial that included cytokine and CMIP expression studies in the same patients at the time of relapse and remission (6). Indeed, we found that MCNS relapses are associated with donwregulation of IL2 concomitantly with an increase in CMIP abundance. Altogether, these findings suggest that CMIP inhibits the differentiation of naïve T cells to effector cells and may be considered as a negative regulator of T-cell signaling. IL-10 plays a key role in preventing inflammatory and autoimmune processes (25). Given the contrasting effects on cytokine production marked by downregulation of IFNγ and IL4 and increased production of IL-10, we postulate that increased Cmip abundance interferes with T cell differentiation into Th1 or Th2 cell subsets, but it may facilitate the development of regulatory T cell response.

Although we focused here on the study of early signaling events in T cells, the findings that Tg T cells were insensitive to PMA/ionomycin activation are unexpected because the

recruitment of proximal signals are classically considered as uncoupled from downstream effectors. Indeed, the inhibitory effects of Cmip seem to involve proximal events occurring in T cell signaling as well as transcriptional machinery leading to cytokine synthesis. The fact that PMA/inomycin-mediated stimulation of IL-4 and IFNγ was sensitive to Cmip inhibition suggests two potential, and not mutually exclusive, mechanisms. The first one relies on cross regulation of factors involved in early T cell proximal events and PKCθ. It has been shown that PKCθ associates with CD28 in PMA stimulated T cells and interacts physically with ZAP70 in lipid rafts, leading to activation of downstream signaling pathways and cytokine synthesis (26). Moreover, PKCθ inhibits the suppressive function of regulatory T cells (27). Whether Cmip can disrupt this regulation loop requires additional investigations. The second mechanism implies a direct effect of Cmip as repressor of NF-kB activity (11, 14). NF-kB binds to CD28 responsive element in the *Il-2* promoter and acts as a potent transactivator (28). Moreover, NF-kB can be activated by stimulation of PKC by PMA (29). The influence of Cmip on the transcriptional regulation of cytokines remains to be investigated.

The most proximal signaling events occurring following T-cell engagement involve the Src family tyrosine kinases Lck and Fyn. The abundance of inactive Src kinases Fyn and Lck is significantly increased following CD3/CD28 stimulation in transgenic T cells, whereas active Src kinase forms assessed by pY^{418}Src are reduced, suggesting that the early molecular events leading to recruitment and activation of Src kinases in LR are altered in the presence of CMIP. Activation of T cells by CD3/CD28 results in the polarization of LR, which are enriched in Src kinases, GPI-linked proteins and adaptor proteins, which function together as signaling platforms. Inasmuch as Lck is required for the tyrosine phosphorylation of CD28 and the recruitment of Zap70, its inactivation affects the early events of proximal signaling, which are critical for migration of T-cell receptors into LR (30). Our results suggest that in transgenic T cells, Lck is maintained in its inactive

conformation, preventing Zap 70 activation and LAT recruitment in LR. We show here that T-cell polarization, as visualized by CTxB, is inhibited after CD3/CD28 stimulation in transgenic T cells, while it is clearly observed in WT T cells. Collectively, these results suggest that CMIP inhibits proximal signaling and prevents the recruitment of LR to the immunological synapse. These two observations -defects in both LR localization of proteins and LR clustering- are complementary. They can be linked, but the information provided by both approaches are independent. CTxB cannot inform about the raft distribution of Src kinases, whereas LR isolation and WB cannot inform about raft clustering at TCR. Altogether, they indicate the existence of an underlying mechanism involving CMIP leading to LR disruption.

Our lipidomic analysis revealed the ganglio-series of glycosphingolipids as the main metabolic pathway impacted by Cmip expression in a cell line model. This finding was consistent with the alterations in membrane raft signaling induced by Cmip expression in T-cells. GM3, the precursor of GM1 and GM2, is the most abundant class of gangliosides in T cells (31), where they seem to play a key role in activation and signal transduction, notably colocalizing with the protein-tyrosine kinase ZAP70 (32). Hence, the observed depleting effect of CMIP expression on GM2 and GM3 cell content and the GM1 localization defect could be fundamental in the inhibition of the immunological synapse formation suggested by our results.

T cell proximal signaling requires the integrity of LR on the following arguments: (1) GM3 is the main component of LR and activation of $CD4^{+}$T cells is severely compromised in G3-deficent mice, highlighting the functional relevance of LR in T cell signaling (33); (2) the clustering of LR occurs at the interphase between T cell and antigen presenting cell, forming the immunonological synapse (34, 35); (3) Lck and Fyn Src kinases, ZAP-70 kinase and adaptors proteins, among others, are recruited to LR (36) and (4) actin

cytoskeleton rearrangement acts as structural regulator of LR dynamics (37). We have previously shown that CMIP interacts physically with Fyn and filamin A so that it may interfere with both LR and cytoskeleton dynamics (13, 38). Altogether, these data suggest that the negative regulatory role of CMIP is complex and may affect early events of T cell signaling. However, the way in which CMIP inhibits LR dynamics by reducing GM3 and GM2 generation remains to be unveiled.

The importance of LR in T-cell activation lies on their ability to promote an efficient recruitment of membrane receptors and proximal protein partners by serving as a signaling platform and to coordinate the rearrangement of actin cytoskeleton, which is required to enable sustained T-cell response activation (39). We sought to understand the impact of CMIP on these molecular events by differential proteomics and found four protein clusters that display significant changes in transgenic T-cells, as compared with WT T cells. We confirmed that cofilin-1, a major mediator of actin dynamics is inactivated in transgenic T cells. It has been shown that T-cell stimulation in the presence of cell-permeable cofilin peptide homologs that inhibit the interaction of cofilin with F-actin filaments results in impaired formation of the immune synapse, reduced production of T helper 1 (Th1) and Th2 cell cytokines, and reduced cell proliferation (23).

CMIP is a new PH and LRR domain-containing protein originally identified in T cells from patients with MCNS disease (5). Several investigations carried out during the last decade shed new light on its structural and functional characteristics (40). Regardless of idiopathic MCNS, the recent observation that CMIP is overproduced in tumor cell environment in patients who develop MCNS in the context of cancer, raises intriguing questions and point out a possible implication of CMIP in the pathophysiological process (9). Until now, we have found that CMIP interacts with multiple partners, interferes with cytoskeletal dynamics, downregulates NF-kB activity and promotes apoptosis (38). Its involvement in

different signaling pathways suggests that CMIP is present in multiple complexes that regulate the response to intracellular and membrane receptors. The current study adds new insight on CMIP function, suggesting a negative regulatory role in T-cell signaling. Negative regulation is critical for the termination of immune responses, for peripheral tolerance, and to prevent inflammation-induced tissue damage. Sustained activation of T lymphocytes resulting from a lack of feedback control can lead to autoimmune diseases, transplant rejection and cancer. Conversely, an excess of negative regulation may impede appropriate T-cell activation in response to pathogens and may lead to chronic infection. In addition, the inability to engage appropriate T-cell response against tumoral neoantigens results in cellular proliferation and metastasis. Indeed, induction of inhibitory molecules such as CTLA-4 and PD-1 is found correlated with the viral load (41), as well as in cancer (42), while their blockade provides a clear survival benefit (43). However, our results do not exclude a role for CMIP as modulator of T cell activation and immune response. Thus, a better understanding of the role of CMIP in the negative regulation of T-cell signaling may open new therapeutic perspectives for manipulation of the immune system.

Materials and Methods

Patients

Ten adult patients were included after informed consent. The diagnosis of MCNS was confirmed by renal biopsy before inclusion. All patients with relapse had proteinuria >3 gr/24h, and low serum albumin levels (<30 gr/L). Blood samples were obtained at the time of diagnosis before any treatment. Remission samples were collected during periods of inactive disease, defined by a proteinuria <0.2g/24 h, without steroid treatment. Samples were obtained in the context of clinical trial (Clinical trial.gouv identifier: NCT01197040) with written consent of participants involved in this study.

Generation of CMIP transgenic mice

A mouse transgenic model was constructed by a targeting system based on reconstitution of functional X-linked hypoxanthine-guanine-phosphorybosyltransferase (Hprt) locus, as previously described (38). The full-length coding sequence of human CMIP was inserted downstream of the distal Lck promoter allowing CMIP expression only in peripheral T-lymphocytes (18). The HPRT PCR product was amplified in WT and heterozygous transgenic female ($Tg^{+/-}$), but not in reconstituted HPRT allele such as in homozygous transgenic female ($Tg^{+/+}$) or hemizygous transgenic male (Tg+) mice. The size of CMIP and HPRT PCR products were 309 and 301 base pairs, respectively (Table S1).

The experimental procedures were approved by the National Ethical Committee (ComEth), under accreditation number 29/01/13-1.

Generation of conditional and inducible T cell specific CMIP Knockout mice. Details of construction of $Cmip^{lox/lox}$ have been previously reported (17). The triple transgenic mouse strain (CD2-rtTA/TetOn-Cre/$CMIP^{loxP/loxP}$) was generated by sequential crossing. We first crossed $Cmip^{lox/lox}$ mice with C.Cg-Tg(tetO-cre)1Jaw/J mice (strain N°006244) that was purchased from Jackson laboratory (Bar Harbor, ME USA). Then, the homozygous double

transgenic TetO-Cre/CmipLox mice were crossed with Tg(CD2-rtTA)CRza mice (a generous gift of R Zamoyska, MRC, London, UK). Offspring were subsequently intercrossed until homozygous mice for the three genes were obtained.

Flow cytometry analysis

Splenocytes were incubated for 10 min at room temperature (RT) with TruStain fcX™ (BioLegend), then stained with anti-mouse fluorochrome-conjugated mAbs against CD4, CD8, CD44, CD62L, 20 min at RT. The CD4-FITC and CD62L-PE antibodies were purchased from Miltenyi Biotech and the CD8-APC and CD44-Pecy7 antibodies were purchased from eBiosciences (Table S2A). Splenocytes were then fixed for 7 min with 4% paraformaldehyde and analyzed by flow cytometry on a FACS analyzer Cyan ADP (Beckman Coulter), using the FlowJo software (Tree Star, San Carlos, CA, USA).

T-cell isolation

Spleens were harvested, gently minced with scalpel and passed through a 40 µM nylon mesh filter. Mononuclear cells were isolated by Ficoll® 400 (Eurobio) density gradient. Purified T cells were isolated by negative selection using the Pan T Cell isolation kit (Miltenyi Biotec GmbH, Germany).

***Ex vivo* T-cell stimulation**

Before stimulation, T cells were systematically synchronized at the G1 phase of cell cycle by serum starvation in 2% fetal calf serum (FCS) for 6 hours. Synchronized T-cells were then activated for the indicated times with soluble anti-CD3 and anti-CD28 (eBiosciences, San Diego, CA, USA) at 1 µg/ml in RPMI complete medium supplemented with 10% FCS. In another set of experiments, T-cells were activated by phorbol 12-myristate 13-acetate (PMA, 50 ng/ml) and ionomycine (0.5 µg/ml) for the indicated times in similar culture

conditions.

Western blot analysis

All primary antibodies used in this study are referenced in Table S2B. Western blots were performed as previously described (38).

Quantification of transcripts by reverse transcription and real time quantitative PCR (RT-qPCR)

Total RNA was extracted and purified using the RNeasy kit (QIAGEN Inc., Germantown, USA), following the supplier's protocol. The sequences of primers are indicated in Table S1. RT-qPCR was performed as previously described (7). All RT-qPCRs were performed in duplicate and normalized to 18S rRNA expression. Cycle thresholds (C_T) were calculated using the relative quantification method (Applied Biosystems). Relative copy numbers were calculated by determining the difference in the C_T between the target and control probes ($\Delta CT = CT_{\text{gene of interest}} - CT_{18S}$)). Cycle thresholds greater than 32 were excluded from analyses. Fold induction of mRNA was evaluated by the $2^{-\Delta\Delta CT}$ method, relative to the unstimulated cells.

T-cell proliferation assay

T-cell proliferation was determined by the extent of carboxyfluorescein diacetate succinimidyl ester (CFSE) dye dilution on culture at day 5 in the presence of soluble anti-CD3/anti-CD28 (1µg/ml each). For CFSE labeling, synchronized T cells were resuspended at 10^7cells/ml in PBS containing 1µM CFSE (eBioscience) and incubated for 10 min at RT. The labeling reaction was stopped by addition of 3 volumes of cold PBS. Then, cells were washed thrice, resuspended in RPMI complete medium supplemented with 10% FCS at 10^7cells/ml, in presence of soluble anti-CD3/CD28 (1 µg/ml), with/wo IL-2 (30 UI/ml) and

incubated for five days. The incorporation of CFSE was measured by flow cytometry.

Immunocytochemistry

T cells were plated at 10^4 cells/slide using a cytospin centrifuge and fixed in 4% PFA for 10 min at RT, then permeabilized by incubation with 0.3% Triton X-100 for 10 min. Endogenous biotin and avidin were blocked using Avidin-Biotin Blocking kit (Vector Laboratories). Membranous ganglioside GM1 was visualized by direct incubation for 25 min at RT with Alexa fluor555-conjugated cholera toxin subunit B (Molecular Probes, 8µg/ml in PBS, 50µl/slide) and washed (3 x 5 min) before being covered with Vectashield mounting containing DAPI (4′,6-diamidino-2-phenylindole) (Vector Laboratories) and viewed under a fluorescence microscope (Zeiss, Germany) with the appropriate filters. To visualize CMIP, a rabbit polyclonal antibody developed in our laboratory was used (1:1000 dilution). The anti-CMIP antibody recognizing both human and mouse CMIP was previously described (17). To ensure the specificity of each signal, IgG isotype control (Cell Signaling) was used instead of primary antibody in control samples.

Confocal and videomicroscopy

All fluorescent images were collected on a Zeiss LSM510 confocal microscope. For live studies, synchronized T cells were stained with AF555-CTB (Molecular Probes, 8µg/ml) and settled onto 8-well ibitreat µ-Slides (Ibidi, Biovalley S.A. France), then stimulated with CD-coated beads (human Dyneabeads CD3, Invitrogen) and soluble anti-CD28 (1µg/ml, eBiosciences) at a 2:1 ratio. One image every 15s was collected. Samples were maintained at 37°C.

Lipid raft preparation

Lipid raft microdomains were obtained by a detergent-free method based on the one

described by McDonald and Pike (44). Between 15 and 30 million cells per sample were washed twice in cold PBS, resuspended in 800µl of MBS/Na_2CO_3 buffer (25mM MES, 150mM NaCl, 250mM Na_2CO_3, pH6; supplemented with 1mM PMSF and phosphatase and protease inhibitor cocktails) and lysed by 20-time passage through a 21G needle, followed by sonicating 3 times for 60 seconds in a Vibra Cell 75022 sonicator. The homogenate was mixed with two volumes of 60% OptiPrep™ (Axis Shield) for a final volume of 2ml of 40% OptiPrep™. A three-step discontinuous density gradient was made by placing 2ml of 30% OptiPrep™ in MBS/Na_2CO_3 buffer, and 1ml of 5% OptiPrep™ sequencially on top of the homogenate. The mixture was spun in a TL-100 rotor at 268,000×g for 2h in an Optima MAX-XP ultracentrifuge (Beckman Coulter). After spinning, 8 fractions of 600µl and a pellet were recovered from top to bottom. For most studies, fractions 2, 3 and 4 and fractions 6, 7 and 8 were pooled separately and labeled as R (raft) and NR (non-rafts), respectively. These pools were characterized using established lipid and protein raft markers, namely Flotillin-1 and cholesterol, respectively. For western blot studies, proteins from R and NR fractions were precipitated by addition of 10% trichloroacetic acid (final concentration), incubation overnight at -20°C and three washes in cold ethanol. The resulting dry protein pellets were solubilized in equal volumes of 5× Laemmli buffer and stored at -80°C until use.

High performance thin layer chromatography (HPTLC)

Cholesterol levels were evaluated by thin layer chromatography as previously described (45). Briefly, R and NR fractions were subjected to organic extraction by addition of 6 volumes of chloroform/methanol (2:1, v/v) and thorough vortexing, followed by centrifugation at 3,000×g for 5min. The organic lower phase was recovered and evaporated to dryness under a nitrogen stream. The dry lipid film was resuspended in 20µl of chloroform/methanol (1:1, v/v). Five µl of each sample were spotted on a Partisil HPK 60Å silica HPTLC plate

(Whatman) along with 3μg of cholesterol standard, pre-developed in chloroform/methanol (1:1, v/v) and developed in chloroform/acetone (95:5, v/v). Bands were detected by dipping the plate into a 626.6mM CuSO4, 8% H_3PO_4 solution followed by charring at 160°C.

Lipid extraction, untargeted lipidomics and analysis of ganglioside metabolism

Untargeted lipidomics was optimized in immortalized mouse podocytes stably transfected with a vector carrying the coding sequence of CMIP or an empty vector as a control. The cell line characteristics and culturing conditions have been described before (38). Five million cells per sample were subjected to organic extraction. Lipids were extracted by adding methanol to dry cell pellets and centrifuged at 10,000xg for10 min at 4°C. The supernatant was then subjected to liquid chromatography−mass spectrometry (LC−MS) analysis using an ionKey/MS system composed of the Acquity UPLC MClass, ionKey source, and an iKey CSH C18 130 Å (1.7 μm particle size) 150 μm × 100 mm column (Waters) coupled to a Synapt G2-Si (Waters). Analyses were conducted with both positive and negative electrospray ionization mode using data-independent acquisition. The capillary voltage was 2.8 kV and the source temperature was 110 °C. Injections were 0.5 μL in the partial-loop mode, with a column temperature of 55 °C and flow rate of 3 μL/min. Mobile phase A consisted of acetonitrile/water (60:40) with 10 mM ammonium formate + 0.1% formic acid. Mobile phase B consisted of 2-propanol/acetonitrile (90:10) with 10 mM ammonium formate + 0.1% formic acid. The gradient was programmed as follows: 0.0−2.0 min, from 40% to 43% B; 2.0−2.1 min, to 50% B; 2.1−12.0 min, to 99% B; 12.0−12.1 min, to 40% B; and 12.1−14.0 min, at 40% B.

Data processing and analysis was conducted using Progenesis QI Informatics (Nonlinear Dynamics, Newcastle, UK) and MetaboAnalyst 3.0 software (46). Each UPLC-MS run was imported as an ion-intensity map, including m/z and retention time. These ion maps were then aligned in the retention-time direction. From the aligned runs, an aggregate run

representing the compounds in all samples was used for peak picking. This aggregate was then compared with all runs, so that the same ions are detected in every run. Isotope and adduct deconvolution was applied, to reduce the number of features detected. Data were normalized according to total ion intensity. Lipids of interested were filtered using ANOVA $p<0.001$ and fold change > 5 for further identification.

Lipids were identified by database searches against their accurate masses using publicly available databases, including Lipid Metabolites and Pathways Strategy (LIPID MAPS) and Human Metabolome database (HMDB), as well as by fragmentation patterns and retention times, when available. Pathway analysis, which consisted of enrichment analysis and pathway topological analysis, were conducted using Metabolomics Pathway Analysis (MetPA) within MetaboAnalyst (47). Additional pathway over-representation analyses were conducted using Integrated Molecular Pathway Level Analysis (IMPaLA) (48).

Proteomic analysis of T cells isolated from WT and transgenic mice

MS/MS protein identification and quantification. Cells were lysed in 2% SDS and boiled at 95°C for 5min. Filter Aided Sample Preparation (FASP) was used for protein digestion. Briefly, cell lysates were treated with 100mM DTT for 30 min at 60°C, mixed with 8M urea buffer, loaded on Microcon 30kDa centrifugal filters (Millipore) and alkylated with 50mM iodoacetamide. Filters were washed twice with 8M urea and twice with 50mM ammonium bicarbonate. Following an overnight trypsin digestion at 37°C, samples were vacuum dried, and resuspended in 10% acetonitrile, 0.1% formic acid, for LC-MS/MS. For each run, 1µg was analysed by nanoRSLC-Q Exactive PLUS MS (Dionex RSLC Ultimate 3000, Thermo Scientific, Waltham, MA, USA). Peptides were separated on a reversed-phase liquid chromatographic column (Pepmap C18, Dionex). Chromatography solvents were (A) 0.1% formic acid in water, and (B) 80% acetonitrile, 0.08% formic acid. Peptides were eluted

from the column with the following gradient: 5% to 40% B (120 min), 40% to 80% (7 minutes). At 127 min, the gradient returned to 5% to re-equilibrate the column for 20 minutes before the next injection. Two blanks, two long 75 min-step gradients, were run between technical and biological triplicates to prevent sample carryover. Peptides eluting from the column were analyzed by data dependent MS/MS, using Top-10 acquisition method. Briefly, the instrument settings were as follows. Resolution was set to 70,000 for MS scans and 17,500 for the data dependent MS/MS scans in order to increase speed. The MS AGC target was set to 3,106 counts, while MS/MS AGC target was set to 5,104. The MS scan range was from 400 to 2000 m/z. MS and MS/MS scans were recorded in profile mode. Dynamic exclusion was set to 30 sec duration. Three replicates of each sample were analyzed by nanoLC/MS/MS.

Data processing following LC-MS/MS acquisition. The raw MS data were processed with the MaxQuant software version 1.5.2.8 and searched with Andromeda search engine against the *Mus musculus* subset of the UniprotKB/Swissprot database (release 2015-03-04, 16704 sequences). To search parent mass and fragment ions, we set search mass deviation of 4.5 ppm and 20 ppm respectively. The minimum peptide length was set to 7 aminoacids and strict specificity for trypsin cleavage was required, allowing up to two missed cleavage sites. Carbamidomethylation (Cys) was set as fixed modification, whereas oxidation (Met) and N-term acetylation were set as variable modifications. The false discovery rates (FDRs) at the protein and peptide level were set to 1%. Scores were calculated in MaxQuant as described previously (49). The reverse and common contaminant hits were removed from MaxQuant output. Proteins were quantified according to the MaxQuant label-free algorithm using LFQ intensities [22,23]; protein quantification was obtained using at least 2 peptides per protein. Statistical and bioinformatic analysis, including heatmaps, profile plots and clustering, were performed with Perseus software (version 1.5.0.31) freely available at

www.perseus-framework.org. For each protein we had LFQ values corresponding to the average LFQ from three technical triplicates. We filtered the data to keep only proteins with at least 5 valid values out of 12. Next, the data were imputed to fill missing data points by creating a Gaussian distribution of random numbers with a standard deviation of 33% relative to the standard deviation of the measured values and 1.8 standard deviation downshift of the mean to simulate the distribution of low signal values. For statistical comparison we performed a two-way ANOVA test, setting 2 groupings: Lck vs Balb/c mice and stimulated versus non-stimulated mice ($p<0.05$). Hierarchical clustering of proteins statistically different between Lck vs Balb/C mice and stimulated versus non-stimulated mice, and of proteins having a significant interaction between the two groupings, were performed in Perseus on logarithmized LFQ intensities after z-score normalization of the data, using Euclidean distances.

Statistical analysis

Data were analyzed with PRISM Software for Macintosh (GraphPad Software, Inc, USA). The difference between the two different groups was determined by using Student t test. P values of less than 0.05 were considered statistically significant.

Supplementary Materials:

1. **Figure S1**. Representative histograms of CFSE fluorescence at Da0 (d0) and day 5 (d5) of WT and Tg T cells stimulated with anti-CD3/CD28 antibodies (1 µg/ml each)

2. **Figure S2.** Effect of PMA/ionomycin stimulation on cytokine expression. T-cells were isolated by negative immunoselection as described in Material and Methods, then activated by phorbol myristate acetate(PMA, 50 ng/ml) and ionomycine (0.5 µg/ml) for the indicated times. IL-2, IL-4, IFNγ and IL-10 transcripts were quantified by RT-qPCR. The results are representative of three independent experiments (n=3 mice in each group). [Tg versus WT, Mean with SD, IL-2: non significant difference (ns); IL-4: 1h-2h: ns, 4h: *p= 0.0476, IFNγ: 1h: *p = 0.019, 2h: ns, 4h: *p = 0.0278; IL-10: 1h-2h: ns, 4h: *p= 0.0476, Mann–Whitney tests].

3. **Figure S3.** Impact of Cmip invalidation on T cell reactivity. **(a-d)** representative Western blots of protein lysates from Cmip-deficient T cells and control littermates T cells, at several times following anti-CD3/CD28 activation (1µg/ml each); blots were striped and reprobed with an antibody raised against total specific protein or a housekeeping gene (GAPDH). The results are representative of three independent experiments [pY^{528}Fyn/total GAPDH: **p= 0.012, KO *vs* Con (30 min); pY^{505}Lck/total Lck: **p= 0.0057, KO *vs* Con (15min); **p= 0.0068, KO *vs* Con (30 min); pY^{418}Src/total Src: *p= 0.0158, KO *vs* Con (15min); **p= 0.0061, KO *vs* Con (30 min); pYr^{319}Zap70/total Zap70, *p= 0.0217, KO *vs* Con (15min); ***p= 0.0008, KO *vs* Con (30 min)]. (**e**) left, genotyping of T cells isolated by negative immunoselection and analysed by PCR from genomic DNA. The bands of 915 bp and 315 bp correspond to $Cmip^{lox/lox}$ and Cmip deletion sequences, respectively

(details of construction are described in reference 17); right, visualization of Cmip by Western blots of protein lysates from Cmip-deficient T cells and control littermates T cells.

4. Data file S1: Pattern of identified signaling pathways
5. Data file S2: Proteomics analysis of WT and transgenic T-cells in resting and following anti-CD3/CD28 stimulation.
6. Data file S3: Differential proteomics analysis of WT and transgenic T-cells in resting and following anti-CD3/CD28 stimulation.
7. Table S1: Oligonucleotides used for genomic DNA and transcript amplification
8. Table S2: Antibody list
9. Movie S1-Videomicroscopy of lipid raft dynamic in WT and transgenic T-cells following anti-CD3/CD28 stimulation (file to open with QuickTime player).

Acknowledgments

We are grateful to Pr Rose Zamoyska (Medical Research Council, London, United Kingdom) for providing us with Tg(CD2-rtTA) CRza mouse model. This work was supported in part by a grant from the French Kidney Foundation. J Oniszczuk**,** P Vachin and K Sendeyo were supported by grants from the Ministry of research.

Author Contributions

JO, KS, CC, PV, BS, EC, CH, VF, AP, GA and ICG performed the experiments. MO, VA and DS wrote the paper. DS and MO supervised the project. All authors discussed the results and participated in writing the paper.

Conflict of interest.

The authors declare that they do not have any competing financial, personal, or professional interests.

References

1. Brubaker SW, Bonham KS, Zanoni I, Kagan JC. Innate immune pattern recognition: a cell biological perspective. Annu Rev Immunol. 2015;33:257-90.

2. Chakraborty AK, Weiss A. Insights into the initiation of TCR signaling. Nat Immunol. 2014;15(9):798-807.

3. Viola A, Gupta N. Tether and trap: regulation of membrane-raft dynamics by actin-binding proteins. Nat Rev Immunol. 2007;7(11):889-96.

4. Brownlie RJ, Zamoyska R. T cell receptor signalling networks: branched, diversified and bounded. Nat Rev Immunol. 2013;13(4):257-69.

5. Sahali D, Pawlak A, Valanciute A, Grimbert P, Lang P, Remy P, et al. A novel approach to investigation of the pathogenesis of active minimal- change nephrotic syndrome using subtracted cDNA library screening. J Am Soc Nephrol. 2002;13(5):1238-47.

6. Boumediene A, Vachin P, Sendeyo K, Oniszczuk J, Zhang SY, Henique C, et al. NEPHRUTIX: A randomized, double-blind, placebo vs Rituximab-controlled trial assessing T-cell subset changes in Minimal Change Nephrotic Syndrome. J Autoimmun. 2018;88:91-102.

7. Sendeyo K, Audard V, Zhang SY, Fan Q, Bouachi K, Ollero M, et al. Upregulation of c-mip is closely related to podocyte dysfunction in membranous nephropathy. Kidney Int. 2013;83(3):414-25.

8. Bouachi K, Moktefi A, Zhang SY, Oniszczuk J, Sendeyo K, Remy P, et al. Expression of CMIP in podocytes is restricted to specific classes of lupus nephritis. PloS one. 2018;13(11):e0207066.

9. Audard V, Zhang SY, Copie-Bergman C, Rucker-Martin C, Ory V, Candelier M, et al. Occurrence of minimal change nephrotic syndrome in classical Hodgkin lymphoma is closely

related to the induction of c-mip in Hodgkin-Reed Sternberg cells and podocytes. Blood. 2010;115(18):3756-62.

10. Bouatou Y, Koessler T, Oniszczuk J, Zhang SY, Moll S, Audard V, et al. Nephrotic Syndrome in Small Cell Lung Cancer and Induction of C-Mip in Podocytes. Am J Kidney Dis. 2017.

11. Kamal M, Valanciute A, Dahan K, Ory V, Pawlak A, Lang P, et al. C-mip interacts physically with RelA and inhibits nuclear factor kappa B activity. Mol Immunol. 2009;46(5):991-8.

12. Kamal M, Pawlak A, BenMohamed F, Valanciute A, Dahan K, Candelier M, et al. C-mip interacts with the p85 subunit of PI3 kinase and exerts a dual effect on ERK signaling via the recruitment of Dip1 and DAP kinase. FEBS Lett. 2010;584(3):500-6.

13. Grimbert P, Valanciute A, Audard V, Lang P, Guellaen G, Sahali D. The Filamin-A is a partner of Tc-mip, a new adapter protein involved in c-maf-dependent Th2 signaling pathway. Mol Immunol. 2004;40(17):1257-61.

14. Izzedine H, Mangier M, Ory V, Zhang SY, Sendeyo K, Bouachi K, et al. Expression patterns of RelA and c-mip are associated with different glomerular diseases following anti-VEGF therapy. Kidney Int. 2014;85(2):457-70.

15. Ory V, Fan Q, Hamdaoui N, Zhang SY, Desvaux D, Audard V, et al. c-mip Down-Regulates NF-kappaB Activity and Promotes Apoptosis in Podocytes. Am J Pathol. 2012;180(6):2284-92.

16. Izzedine H, Escudier B, Lhomme C, Pautier P, Rouvier P, Gueutin V, et al. Kidney diseases associated with anti-vascular endothelial growth factor (VEGF): an 8-year observational study at a single center. Medicine (Baltimore). 2014;93(24):333-9.

17. Moktefi A, Zhang SY, Vachin P, Ory V, Henique C, Audard V, et al. Repression of CMIP transcription by WT1 is relevant to podocyte health. Kidney Int. 2016;90(6):1298-311.

18. Nakao A, Miike S, Hatano M, Okumura K, Tokuhisa T, Ra C, et al. Blockade of transforming growth factor beta/Smad signaling in T cells by overexpression of Smad7 enhances antigen-induced airway inflammation and airway reactivity. J Exp Med. 2000;192(2):151-8.

19. Ballarin-Gonzalez B, Dagnaes-Hansen F, Fenton RA, Gao S, Hein S, Dong M, et al. Protection and Systemic Translocation of siRNA Following Oral Administration of Chitosan/siRNA Nanoparticles. Mol Ther Nucleic Acids. 2013;2:e76.

20. Gao S, Dagnaes-Hansen F, Nielsen EJ, Wengel J, Besenbacher F, Howard KA, et al. The effect of chemical modification and nanoparticle formulation on stability and biodistribution of siRNA in mice. Mol Ther. 2009;17(7):1225-33.

21. Malissen B, Bongrand P. Early T cell activation: integrating biochemical, structural, and biophysical cues. Annu Rev Immunol. 2015;33:539-61.

22. Zeng P, Xu Y, Zeng C, Ren H, Peng M. Chitosan-modified poly(D,L-lactide-co-glycolide) nanospheres for plasmid DNA delivery and HBV gene-silencing. Int J Pharm. 2011;415(1-2):259-66.

23. Eibert SM, Lee KH, Pipkorn R, Sester U, Wabnitz GH, Giese T, et al. Cofilin peptide homologs interfere with immunological synapse formation and T cell activation. Proc Natl Acad Sci U S A. 2004;101(7):1957-62.

24. Yu L, Ye J, Liu Q, Feng J, Gu X, Sun Q, et al. cMaf inducing protein inhibits cofilin1 activity and alters podocyte cytoskeleton organization. Molecular medicine reports. 2017;16(4):4955-63.

25. Saraiva M, O'Garra A. The regulation of IL-10 production by immune cells. Nat Rev Immunol. 2010;10(3):170-81.

26. Xie J, Han X, Zhao C, Canonigo-Balancio AJ, Yates JR, 3rd, Li Y, et al. Phosphotyrosine-dependent interaction between the kinases PKCtheta and Zap70 promotes

proximal TCR signaling. Sci Signal. 2019;12(577).

27. Zanin-Zhorov A, Ding Y, Kumari S, Attur M, Hippen KL, Brown M, et al. Protein kinase C-theta mediates negative feedback on regulatory T cell function. Science. 2010;328(5976):372-6.

28. Ghosh P, Tan TH, Rice NR, Sica A, Young HA. The interleukin 2 CD28-responsive complex contains at least three members of the NF kappa B family: c-Rel, p50, and p65. Proc Natl Acad Sci U S A. 1993;90(5):1696-700.

29. Bomsztyk K, Rooney JW, Iwasaki T, Rachie NA, Dower SK, Sibley CH. Evidence that interleukin-1 and phorbol esters activate NF-kappa B by different pathways: role of protein kinase C. Cell Regul. 1991;2(4):329-35.

30. Zamoyska R, Basson A, Filby A, Legname G, Lovatt M, Seddon B. The influence of the src-family kinases, Lck and Fyn, on T cell differentiation, survival and activation. Immunol Rev. 2003;191:107-18.

31. Tuosto L, Parolini I, Schroder S, Sargiacomo M, Lanzavecchia A, Viola A. Organization of plasma membrane functional rafts upon T cell activation. Eur J Immunol. 2001;31(2):345-9.

32. Garofalo T, Lenti L, Longo A, Misasi R, Mattei V, Pontieri GM, et al. Association of GM3 with Zap-70 induced by T cell activation in plasma membrane microdomains: GM3 as a marker of microdomains in human lymphocytes. J Biol Chem. 2002;277(13):11233-8.

33. Nagafuku M, Okuyama K, Onimaru Y, Suzuki A, Odagiri Y, Yamashita T, et al. CD4 and CD8 T cells require different membrane gangliosides for activation. Proc Natl Acad Sci U S A. 2012;109(6):E336-42.

34. Dykstra M, Cherukuri A, Sohn HW, Tzeng SJ, Pierce SK. Location is everything: lipid rafts and immune cell signaling. Annu Rev Immunol. 2003;21:457-81.

35. Davis DM, Dustin ML. What is the importance of the immunological synapse? Trends

Immunol. 2004;25(6):323-7.

36. Zumerle S, Molon B, Viola A. Membrane Rafts in T Cell Activation: A Spotlight on CD28 Costimulation. Frontiers in immunology. 2017;8:1467.

37. Ballek O, Valecka J, Dobesova M, Brouckova A, Manning J, Rehulka P, et al. TCR Triggering Induces the Formation of Lck-RACK1-Actinin-1 Multiprotein Network Affecting Lck Redistribution. Frontiers in immunology. 2016;7:449.

38. Zhang SY, Kamal M, Dahan K, Pawlak A, Ory V, Desvaux D, et al. c-mip impairs podocyte proximal signaling and induces heavy proteinuria. Sci Signal. 2010;3(122):ra39.

39. Varshney P, Yadav V, Saini N. Lipid rafts in immune signalling: current progress and future perspective. Immunology. 2016;149(1):13-24.

40. Sahali D, Sendeyo K, Mangier M, Audard V, Zhang SY, Lang P, et al. Immunopathogenesis of idiopathic nephrotic syndrome with relapse. Semin Immunopathol. 2014;36(4):421-9.

41. Kassu A, Marcus RA, D'Souza MB, Kelly-McKnight EA, Golden-Mason L, Akkina R, et al. Regulation of virus-specific CD4+ T cell function by multiple costimulatory receptors during chronic HIV infection. J Immunol. 2010;185(5):3007-18.

42. Hodi FS, Mihm MC, Soiffer RJ, Haluska FG, Butler M, Seiden MV, et al. Biologic activity of cytotoxic T lymphocyte-associated antigen 4 antibody blockade in previously vaccinated metastatic melanoma and ovarian carcinoma patients. Proc Natl Acad Sci U S A. 2003;100(8):4712-7.

43. Velu V, Titanji K, Zhu B, Husain S, Pladevega A, Lai L, et al. Enhancing SIV-specific immunity in vivo by PD-1 blockade. Nature. 2009;458(7235):206-10.

44. Macdonald JL, Pike LJ. A simplified method for the preparation of detergent-free lipid rafts. J Lipid Res. 2005;46(5):1061-7.

45. Bourderioux M, Nguyen-Khoa T, Chhuon C, Jeanson L, Tondelier D, Walczak M, et

al. A new workflow for proteomic analysis of urinary exosomes and assessment in cystinuria patients. Journal of proteome research. 2015;14(1):567-77.

46. Xia J, Mandal R, Sinelnikov IV, Broadhurst D, Wishart DS. MetaboAnalyst 2.0--a comprehensive server for metabolomic data analysis. Nucleic Acids Res. 2012;40(Web Server issue):W127-33.

47. Li F, Xu Y, Shang D, Yang H, Liu W, Han J, et al. MPINet: metabolite pathway identification via coupling of global metabolite network structure and metabolomic profile. BioMed research international. 2014;2014:325697.

48. Cavill R, Kamburov A, Ellis JK, Athersuch TJ, Blagrove MS, Herwig R, et al. Consensus-phenotype integration of transcriptomic and metabolomic data implies a role for metabolism in the chemosensitivity of tumour cells. PLoS computational biology. 2011;7(3):e1001113.

49. Cox J, Mann M. MaxQuant enables high peptide identification rates, individualized p.p.b.-range mass accuracies and proteome-wide protein quantification. Nature biotechnology. 2008;26(12):1367-72.

Legends

Figure 1. Expression of CMIP in MCNS. (**a**) RT-qPCR of CMIP expression in healthy subjects (n=10) and MCNS patients (n=10) at the time of relapse then in steroid-free remission. Quantification is measured as -fold induction relatively to control subject. (Mean with SEM, *p= 0.0156, Mann–Whitney test). (**b**) Western blot analysis of CMIP expression in PBMC of MCNS patients in relapse and remission. Positive control consists of recombinant human CMIP transfected in HEK cells. (**c**) Confocal microscopy analysis of MCNS T cells from relapse, isolated by negative immunoselection and double-labeled with CMIP (green) and CD3 (red) antibodies.

Figure 2. Generation of CMIP transgenic mice. (**a**) Schematic diagram of targeted transgenesis into the HPRT locus (see detail in Materials and Methods). All mice analyzed in this study were hemizygous males from F10 to F18 generations. (**b**) PCR genotyping of mouse tail DNA. The HPRT PCR product is amplified in WT allele, but not in reconstituted HPRT gene such as in homozygous transgenic female (Tg+/+) or hemizygous transgenic male (Tg+). (**c**) Quantification of mouse and human CMIP transcripts in transgenic mice and WT by RT-qPCR. (**d**) Confocal immunofluorescence microscopy of CMIP expression in T cells from WT and transgenic. The most right figure of the panel corresponds to negative control, using IgG isotype control instead of primary antibody (Cmip/CD4) in Tg T cells.

Figure 3. Transgenic mice develop an altered T-cell phenotype. (**a**) and (**b**) Representative flow cytometry analysis of naïve, effector and memory T cells in transgenic and WT T cells. Splenocytes from 12-week old transgenic mice (Tg) and WT were gated for CD4+ cells (**a**) or for CD8+ cells (**b**) and analyzed for CD44 and CD62L expression. T-cell

subpopulations were defined as naive ($CD44^{low/verylow}CD62L^{high}$), memory ($CD44^{high}CD62L^{high}$), or effector T cells ($CD44^{high}CD62L^{low}$). The numbers inside and outside each small square indicate respectively the percentage and the absolute number of cells. The total number of events is shown at the top. (**c**) and (**d**) Frequency of naïve, effector and memory T cells. Results are representative of three independent experiments (n=5 for WT and transgenic mice in each). The frequency of naive T-cells in both CD4+ and CD8+ compartments was significantly increased, whereas the level of memory CD4+ was decreased in transgenic mice comparatively to WT (Tg versus WT, Mean with SEM: naïve CD4+, **p= 0.0079; naïve CD8+, p= 0.0159; memory CD4+, p= 0.0303, Mann–Whitney test). Although effector CD+ and CD8+ subsets are decreased in Tg mice, they do not reach statistical significance. (**e**) Transgenic T cells exhibit a lower proliferative capacity. T cells were isolated from Tg mice and WT and labeled with CFSE (1μM). After synchronization, cells were stimulated with anti-CD3/CD28 antibodies (1μg/ml each). After 5 days, proliferation was analyzed by flow cytometry as the percentage of dividing cells. Addition of mouse recombinant IL2 (30U/mL), at 24 and 72 hours post stimulation, restores T-cell proliferation rate at comparable level between Tg mice and WT. Data are presented as the mean of four independent experiments. (Tg versus WT at day 5, Mean with SD: * p= 0.0286, Mann–Whitney test).

Figure 4. Influence of CMIP induction on cytokine expression. (**a**) Expression of CMIP transcript. Total RNA was extracted from synchronized T cells before and after CD3/CD28 stimulation (1μg/ml each) at the indicated times. The expression od endogenous Cmip in WT (green) and Tg mice (bleue), along with Tg Cmip (red) is shown. (**b**) Expression of CMIP protein in same conditions. (**c**) IL-2, IFNγ, IL-4 and IL-10 transcripts were quantified by RT-qPCR. The results are representative of three independent experiments (n=5 mice in each group). [Tg versus WT, Mean with SEM, IL-2, 1h: *p= 0.0278, 2h: **p=

0.0040, 4h: **p= 0.0040; IL-4, 1h: **p= 0.0040, 2h: **p= 0,0040, 4h: **p= 0,0040, 6h: *p= 0.0278, 8 and 16 h: no significant (ns); IFNγ, 1h: *p= 0.0257, 2h: **p= 0.0040, 4h: **p= 0.0079, 6h: *p= 0.0317, 8h: *p= 0.0317 and 16 h: p= 0.532 (ns); IL-10, 1h: *p= 0.0286, 2h: *p= 0.0159, 4h: p= 0.1508 (ns), 6h: *p= 0.0159, 8h: **p= 0.0079, 16h: **p= 0.0079, Mann–Whitney tests].

Figure 5. Transgenic T cells exhibit a hypophosphorylated protein profile with downregulation of active Src. (**a**) Representative Western blot of anti-phosphotyrosine 4G10 on protein lysates from transgenic and WT T cells, after 60 min activation by anti-CD3/CD28; blots were striped and reprobed with anti-GAPDH antibody. (**b**-**e**) Western blots of protein lysates from transgenic and WT T cells, at several times following anti-CD3/CD28 activation (1µg/ml each); blots were striped and reprobed with an antibody raised against total specific protein. The results are representative of three independent experiments [pY^{418}Src/total Src: one-way ANOVA, *p= 0.0163; pY^{505}Lck/total Lck: Kruskal-Wallis test, *p= 0.0362; pY^{528}Fyn/total GAPDH, one-way ANOVA, *p= 0.0204, Tg *vs* WT (30 min), **p= 0.0015; pYr^{319}Zap70/total Zap70, **p= 0.0068]. (**f**) Immunofluorescence staining of pY^{418}Src in transgenic and WT T cells isolated by negative immunoselection.

Figure 6. Transgenic T cell exhibit higher level of inactive Fyn and Lck in LR and fail to be activated after CD3/CD28 costimulation. (**a**) Western blot and TLC in rafts (R) and non-raft (NR) fractions prepared from resting (0 min) and activated (30 min) transgenic and WT T cells. Rafts are enriched in Flotillin-1 and cholesterol. Samples were analyzed with anti-pY^{528}Fyn and anti-pY^{505}Lck antibodies, recognizing the inactive forms, followed by antibodies recognizing the total forms of Fyn and Lck respectively. Cholesterol was analyzed by TLC. (**b**) and (**c**), inactive/total Fyn and inactive/total Lck ratios in raft

microdomains according to densitometric analysis of bands shown in A.

Figure 7. CMIP inhibits clustering and activation of raft signaling platform. (**a**) CMIP inhibits membrane clustering of Src kinases and CTB after CD3/CD28 stimulation. Immunofluorescence analysis of transgenic and WT T cells after 30 min activation by anti-CD3/CD28 antibodies (1 μg/ml each), then fixed and immunostained for total Src (green) and CTB (red). Cell nuclei were revealed by counterstaining with DAP dye. Confocal analysis shows that Src kinases and CTB co-localize in WT but not in transgenic T cells. (**b**) CMIP inhibits clustering into LR of LAT and CTB, after CD3/CD28 stimulation. Fluorescence analysis of LAT and CTB after similar T-cell activation than (**a**). (**c**) negative controls of Src, LAT and CTB: the specificity of each signal was assessed using IgG isotype control instead of primary antibody in WT T cells. (**d**) CMIP inhibits LR clustering and T-cell polarization. Transgenic and WT T cells were synchronized, stained with CTB, loaded into 8-well plates at 50000c/well and activated with anti-CD3-coated beads (ratio cells:beads, 2:1) and soluble anti-CD28 (1μg/ml). Cells were kept at 37°C. Data were acquired in a confocal microscope at 1 image/ 15 sec. Images were extracted from movies (1 image/ 1 min) and analyzed by Image J software (magnification: 63x)

Figure 8. CMIP induces alterations in the glycosphingolipid biosynthetic pathway and in ganglioside species. A mouse podocyte cell line was stably transfected with a CMIP expression vector or with an empty vector (EV). Lipids were extracted and subjected to LC-MS analysis. (**a**) Principal component analysis of ion abundance in the positive and negative modes was able to discriminate CMIP-transfected and EV-transfected cells. PC1 accounted for 74.6% of total variance. (**b**) Metabolome view after MetPA shows sphingolipid metabolism as the most significantly altered pathway by CMIP expression. Total: the total number of compounds in the pathway; Hits: the actually matched number

from the uploaded data; Raw p: original p value calculated from the enrichment analysis; Holm p: p value adjusted by Holm-Bonferroni method; FDR p: p value adjusted using False Discovery Rate; Impact: pathway impact value calculated from pathway topology analysis. (**c**) Relative abundance of several ganglioside species showing a very significant difference between empty vector-transfected and CMIP- transfected cells. Data are expressed as means ± SD of normalized arbitrary units. ***p<0.001. EV: n=3. CMIP: n=6. (**d**) Representative Western blot of GM3 synthase (*St3Gal5* gene) on protein lysates from resting (0 min) or 30 and 60 min anti-CD3/CD28 activation of transgenic and WT T cells; blots were striped and reprobed with anti-GAPDH antibody. Statistical analyses were performed from three independent experiments [Tg *vs* WT (30 min), ***p= 0.0005 and Tg *vs* WT (60 min), *p= 0.0254)].

Figure 9. Impact of CMIP expression and T-cell activation on total proteome. (**a**) Heat map showing the 46 proteins differentially expressed in T-cells obtained from transgenic and WT mice and subjected or not to 60 min costimulation by anti-CD3 /CD28 antibodies (1µg/ml each). The column tree denote the mice grouped by hierarchical clustering. Rows correspond to 46 proteins differentially expressed according to two-way ANOVA analysis (p<0.01), distributed into four clusters. Each cluster corresponds to proteins showing a similar variation pattern depending on both parameters (CMIP expression and T-cell activation). Proteins are labeled using their gene acronyms. (**b**) Phosphorylation/inactivation of Cofilin-1 in transgenic T-cells. Western blot for cofilin-1 from total extracts of transgenic and WT T-cells isolated by negative immunoselection, in resting conditions (0 min) and after 15 or 60 min costimulation with anti-CD3/CD28 antibodies (1 µg/ml each). Samples were analyzed with an anti-pSer3-Cofilin-1 antibody, recognizing the inactive form, and by an antibody recognizing the total form of Cofilin-1.

GAPDH was used as a load control. The right panel shows the inactive/total Cofilin-1 ratio, according to densitometric analysis.

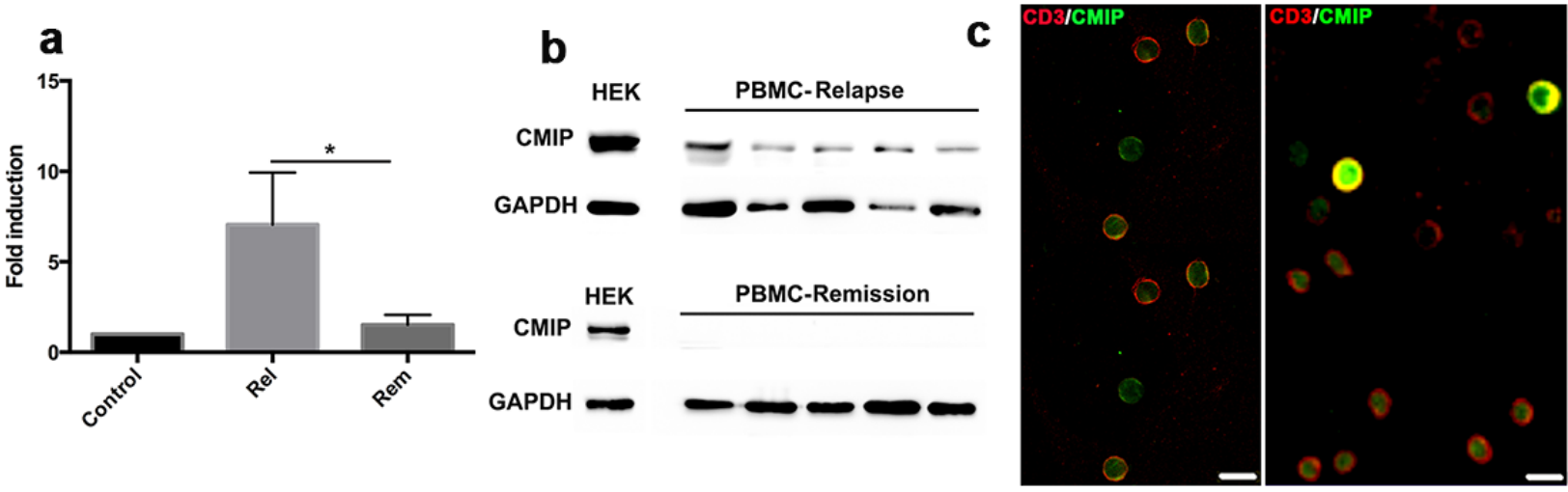
a
Fold induction
15
10
5
0
*
Control
Rel
Rem
b
HEK
PBMC-Relapse
CMIP
GAPDH
HEK
PBMC-Remission
CMIP
GAPDH
c
CD3/CMIP
CD3/CMIP

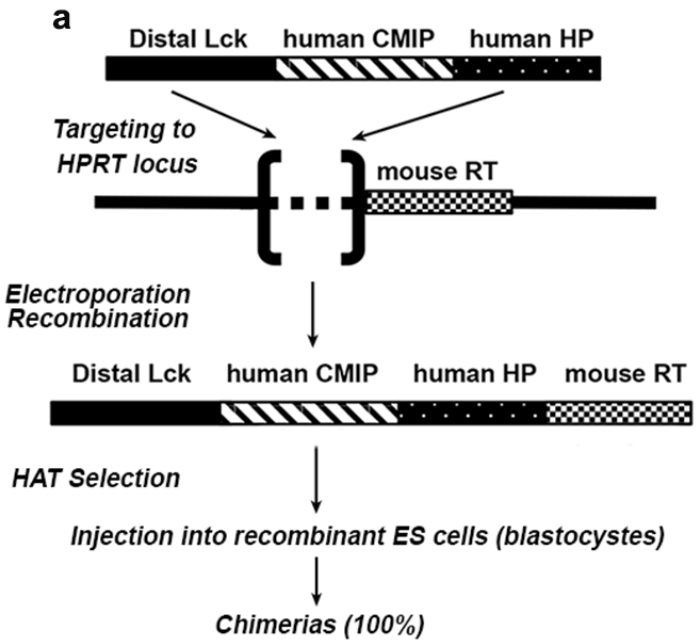
a
Distal Lck
human CMIP
human HP
Targeting to
HPRT locus
mouse RT
Electroporation
Recombination
Distal Lck
human CMIP
human HP
mouse RT
HAT Selection
Injection into recombinant ES cells (blastocystes)
Chimerias (100%)

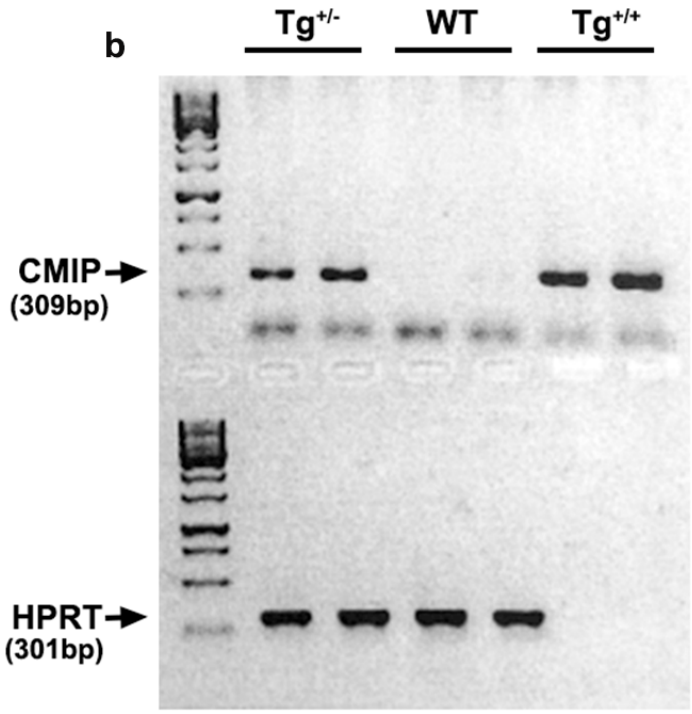
b
Tg+/-
WT
Tg+/+
CMIP
(309bp)
HPRT
(301bp)

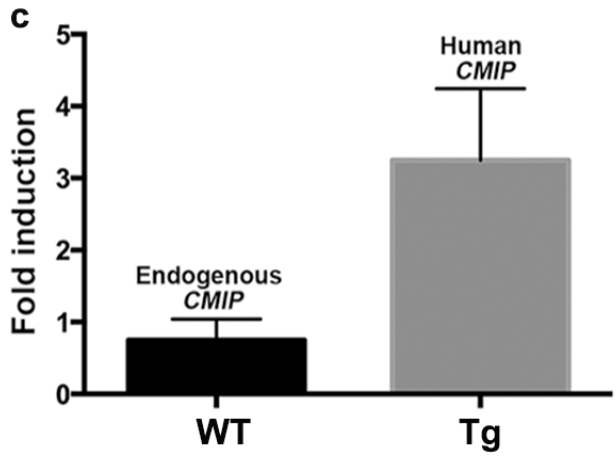
c
Fold induction
0
1
2
3
4
5
Endogenous
CMIP
Human
CMIP
WT
Tg

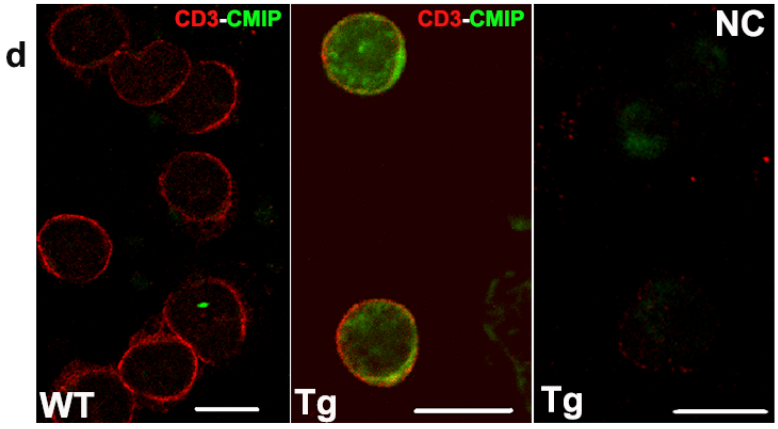
d
CD3-CMIP
CD3-CMIP
NC
WT
Tg
Tg

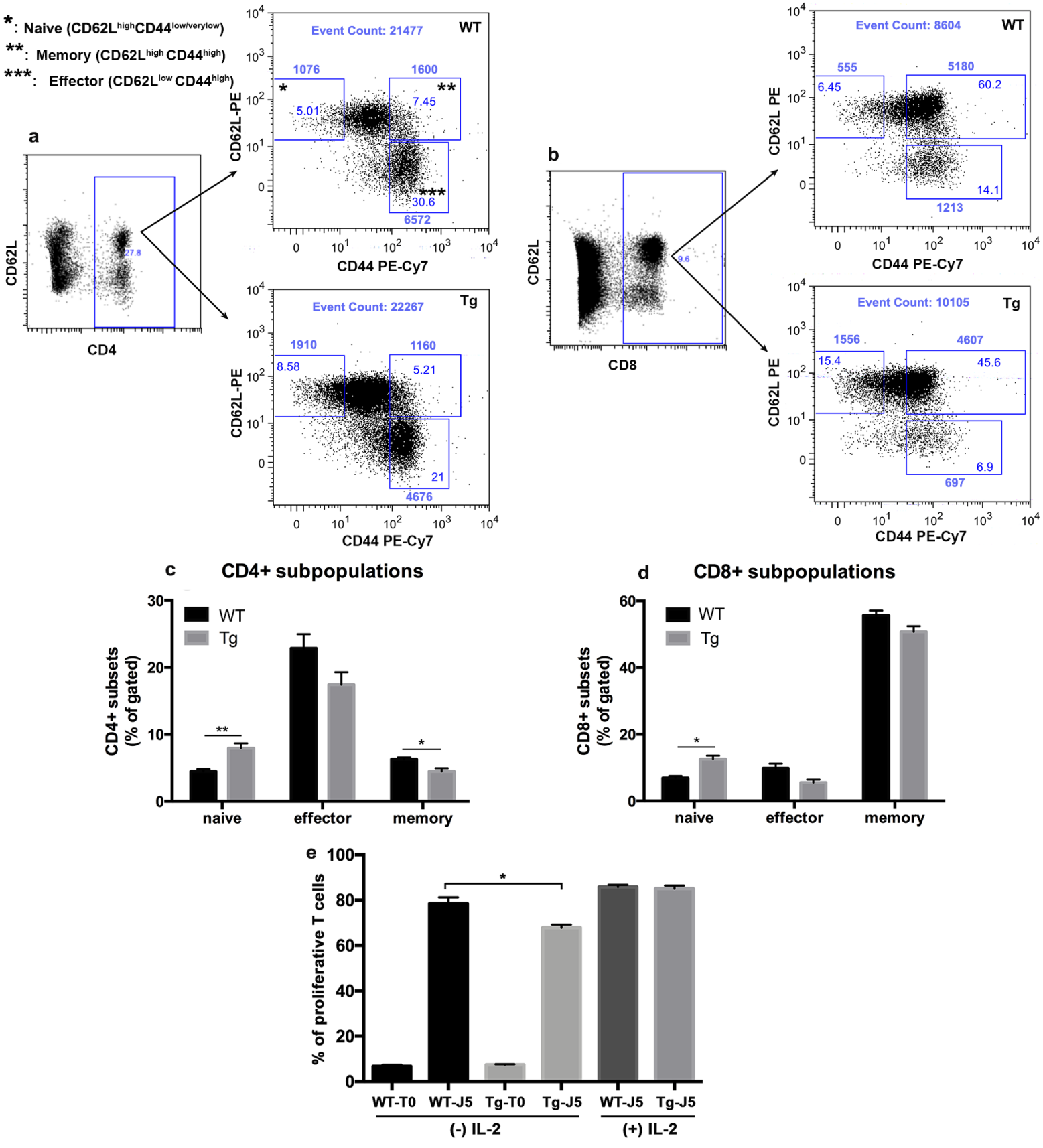
*: Naive (CD62L^high CD44^low/verylow)
**: Memory (CD62L^high CD44^high)
***: Effector (CD62L^low CD44^high)
a
CD62L
CD4
27.8
CD62L-PE
CD44 PE-Cy7
Event Count: 21477
WT
1076
1600
5.01
7.45
30.6
6572
Event Count: 22267
Tg
1910
1160
8.58
5.21
21
4676
b
CD8
9.6
CD62L PE
Event Count: 8604
555
5180
6.45
60.2
14.1
1213
Event Count: 10105
1556
4607
15.4
45.6
6.9
697
c
CD4+ subpopulations
CD4+ subsets (% of gated)
WT
Tg
naive
effector
memory
d
CD8+ subpopulations
CD8+ subsets (% of gated)
e
% of proliferative T cells
WT-T0
WT-J5
Tg-T0
Tg-J5
(-) IL-2
(+) IL-2

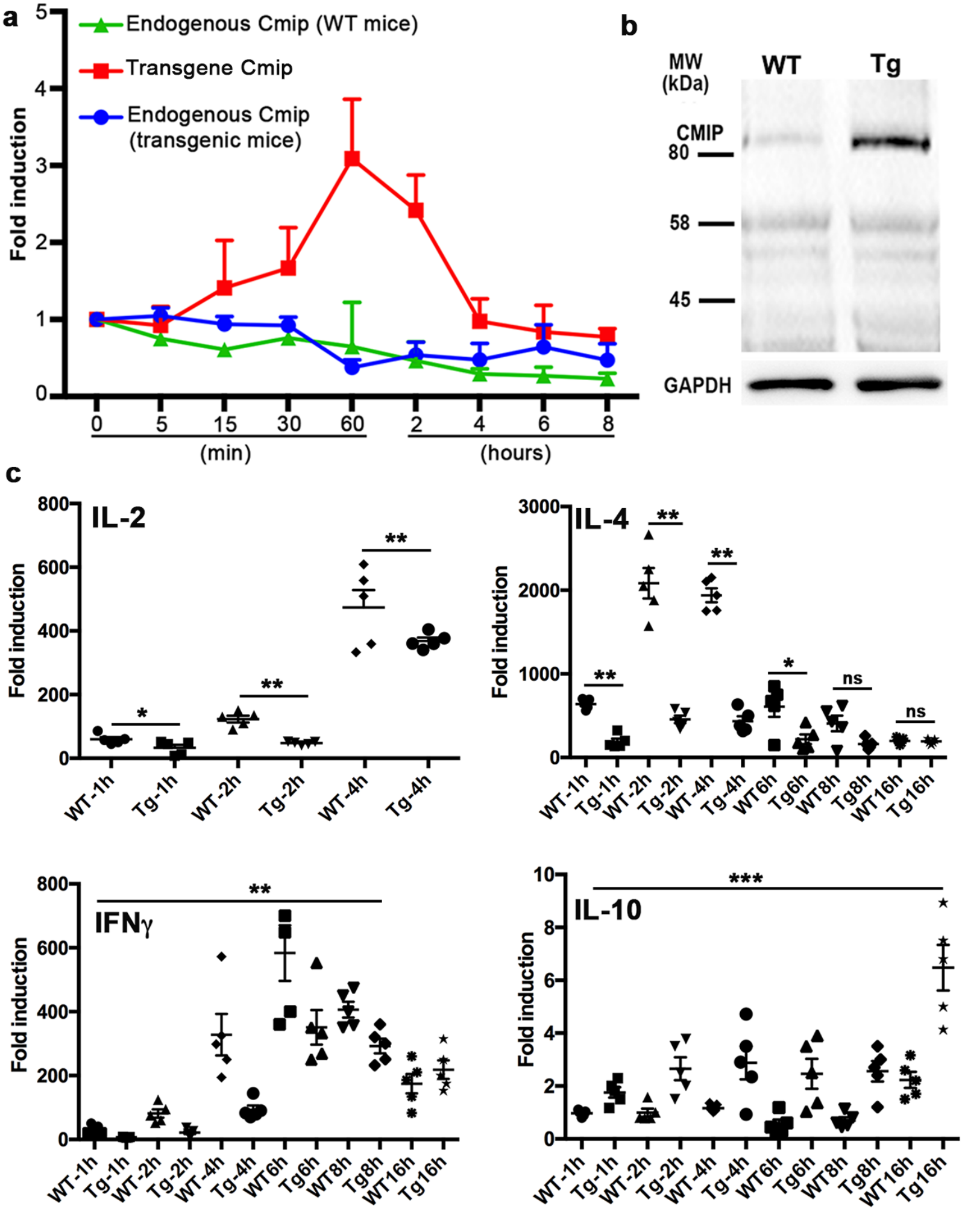
a
Endogenous Cmip (WT mice)
Transgene Cmip
Endogenous Cmip (transgenic mice)
Fold induction
0
1
2
3
4
5
0
5
15
30
60
2
4
6
8
(min)
(hours)
b
MW (kDa)
WT
Tg
CMIP
80
58
45
GAPDH
c
IL-2
Fold induction
800
600
400
200
0
*
**
**
WT-1h
Tg-1h
WT-2h
Tg-2h
WT-4h
Tg-4h
IL-4
3000
2000
1000
0
**
**
**
*
ns
ns
WT-1h
Tg-1h
WT-2h
Tg-2h
WT-4h
Tg-4h
WT6h
Tg6h
WT8h
Tg8h
WT16h
Tg16h
IFNγ
800
600
400
200
0
**
WT-1h
Tg-1h
WT-2h
Tg-2h
WT-4h
Tg-4h
WT6h
Tg6h
WT8h
Tg8h
WT16h
Tg16h
IL-10
10
8
6
4
2
0
***
WT-1h
Tg-1h
WT-2h
Tg-2h
WT-4h
Tg-4h
WT6h
Tg6h
WT8h
Tg8h
WT16h
Tg16h

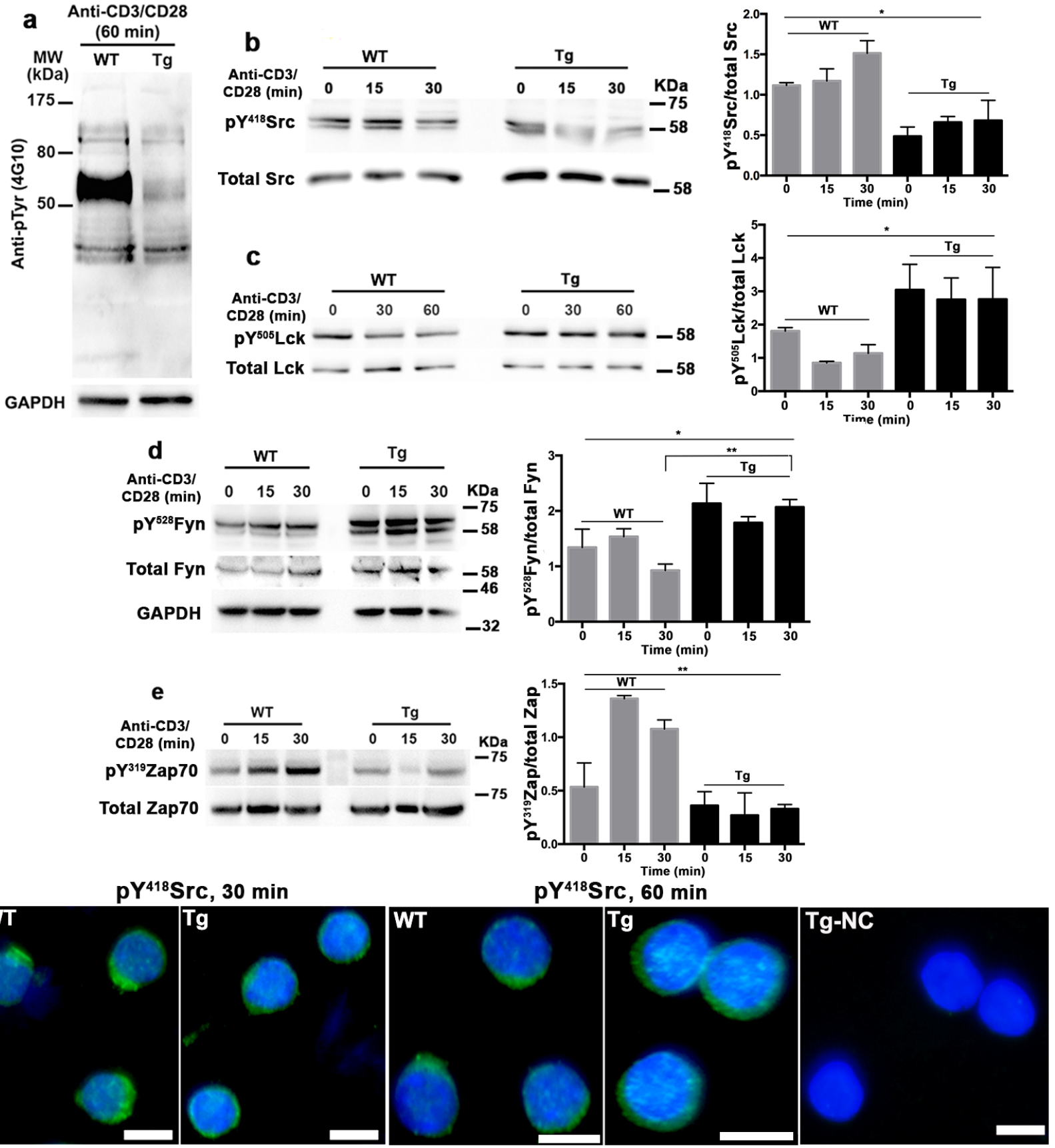
a
Anti-CD3/CD28
(60 min)
MW
(kDa)
WT
Tg
175
80
50
Anti-pTyr (4G10)
GAPDH
b
WT
Tg
Anti-CD3/
CD28 (min)
0
15
30
0
15
30
KDa
75
pY418Src
58
Total Src
58
pY418Src/total Src
2.0
1.5
1.0
0.5
0.0
*
WT
Tg
0
15
30
0
15
30
Time (min)
c
WT
Tg
Anti-CD3/
CD28 (min)
0
30
60
0
30
60
pY505Lck
58
Total Lck
58
pY505Lck/total Lck
5
4
3
2
1
0
*
Tg
WT
0
15
30
0
15
30
Time (min)
d
WT
Tg
Anti-CD3/
CD28 (min)
0
15
30
0
15
30
KDa
pY528Fyn
75
58
Total Fyn
58
46
GAPDH
32
pY528Fyn/total Fyn
3
2
1
0
*
**
Tg
WT
0
15
30
0
15
30
Time (min)
e
WT
Tg
Anti-CD3/
CD28 (min)
0
15
30
0
15
30
KDa
pY319Zap70
75
Total Zap70
75
pY319Zap/total Zap
1.5
1.0
0.5
0.0
**
WT
Tg
0
15
30
0
15
30
Time (min)
f
pY418Src, 30 min
pY418Src, 60 min
WT
Tg
WT
Tg
Tg-NC

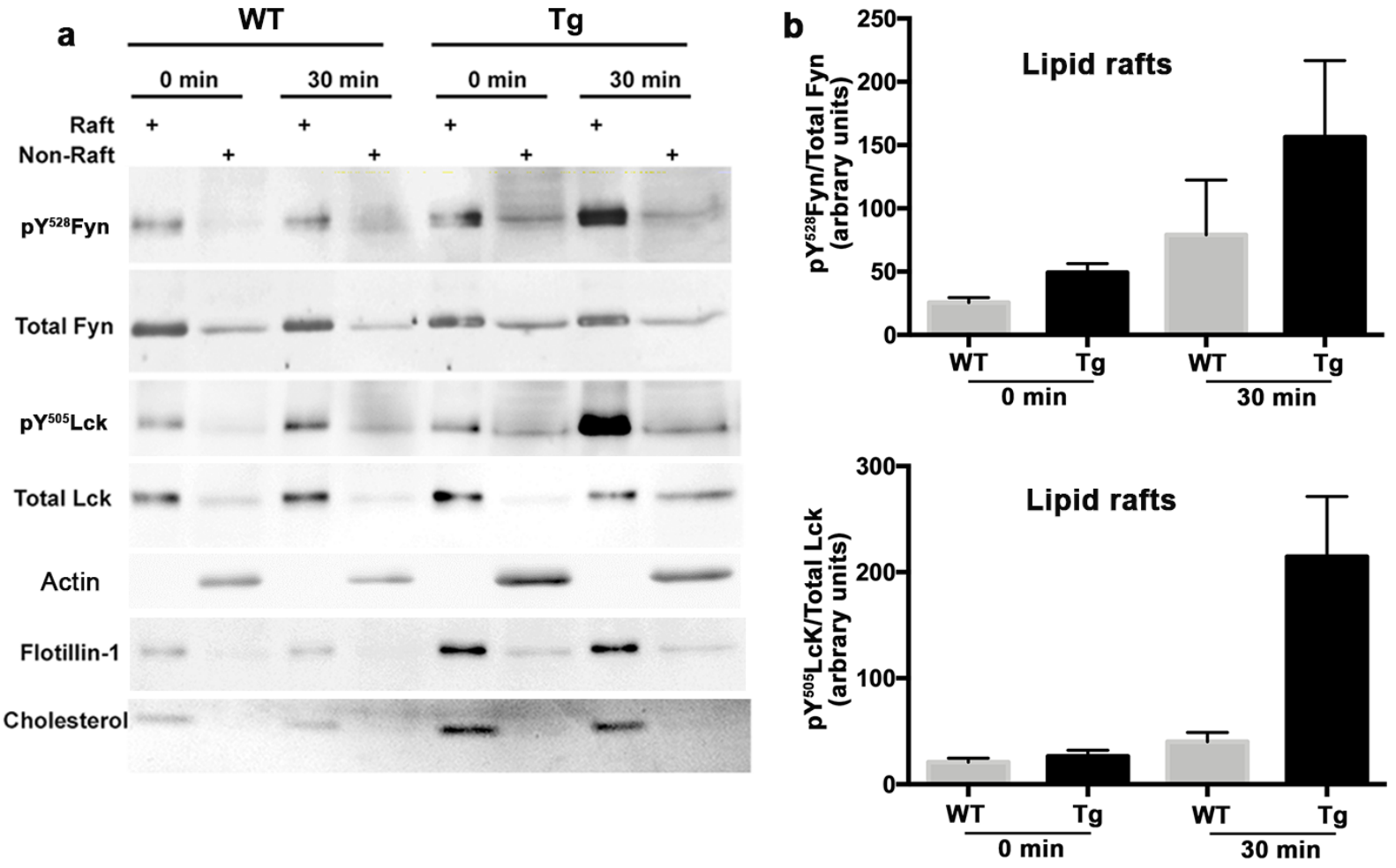
a
WT
Tg
0 min
30 min
0 min
30 min
Raft
Non-Raft
pY528Fyn
Total Fyn
pY505Lck
Total Lck
Actin
Flotillin-1
Cholesterol
b
Lipid rafts
pY528Fyn/Total Fyn (arbrary units)
250
200
150
100
50
0
WT
Tg
WT
Tg
0 min
30 min
Lipid rafts
pY505LcK/Total Lck (arbrary units)
300
200
100
0
WT
Tg
WT
Tg
0 min
30 min

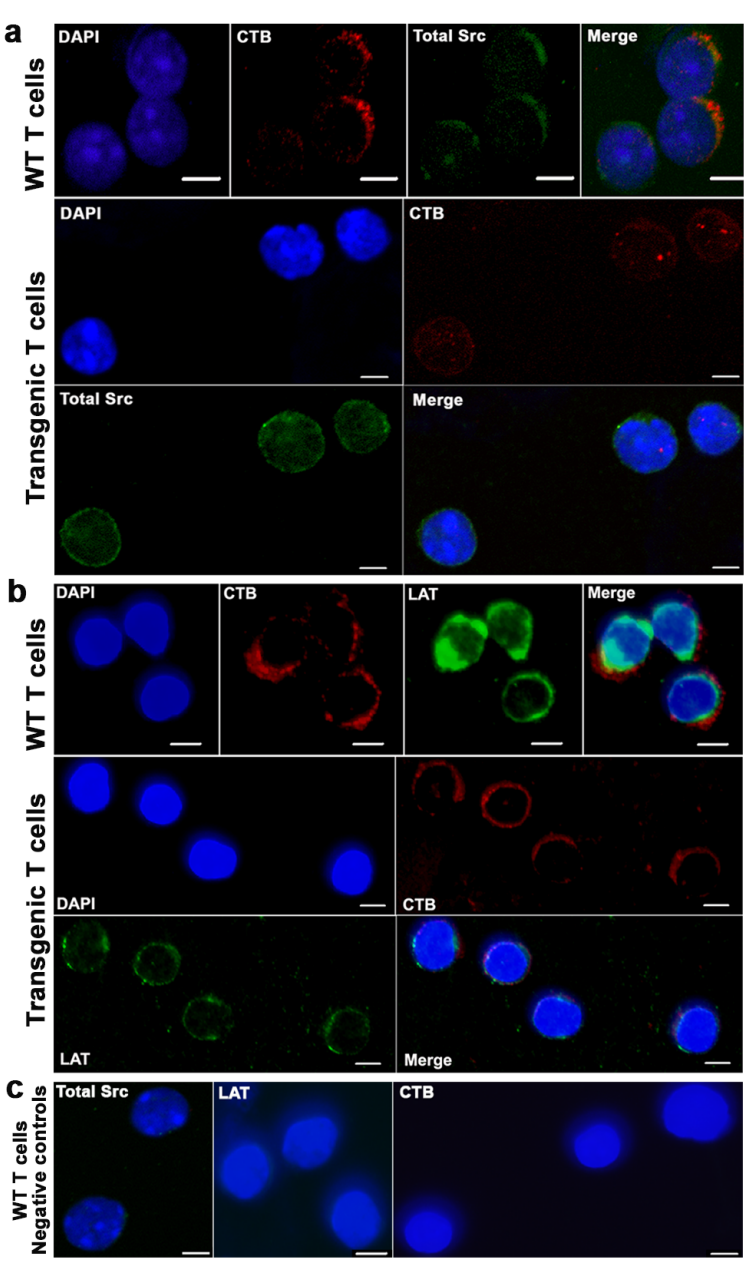
a
WT T cells
DAPI
CTB
Total Src
Merge
Transgenic T cells
DAPI
CTB
Total Src
Merge
b
WT T cells
DAPI
CTB
LAT
Merge
Transgenic T cells
DAPI
CTB
LAT
Merge
c
WT T cells
Negative controls
Total Src
LAT
CTB

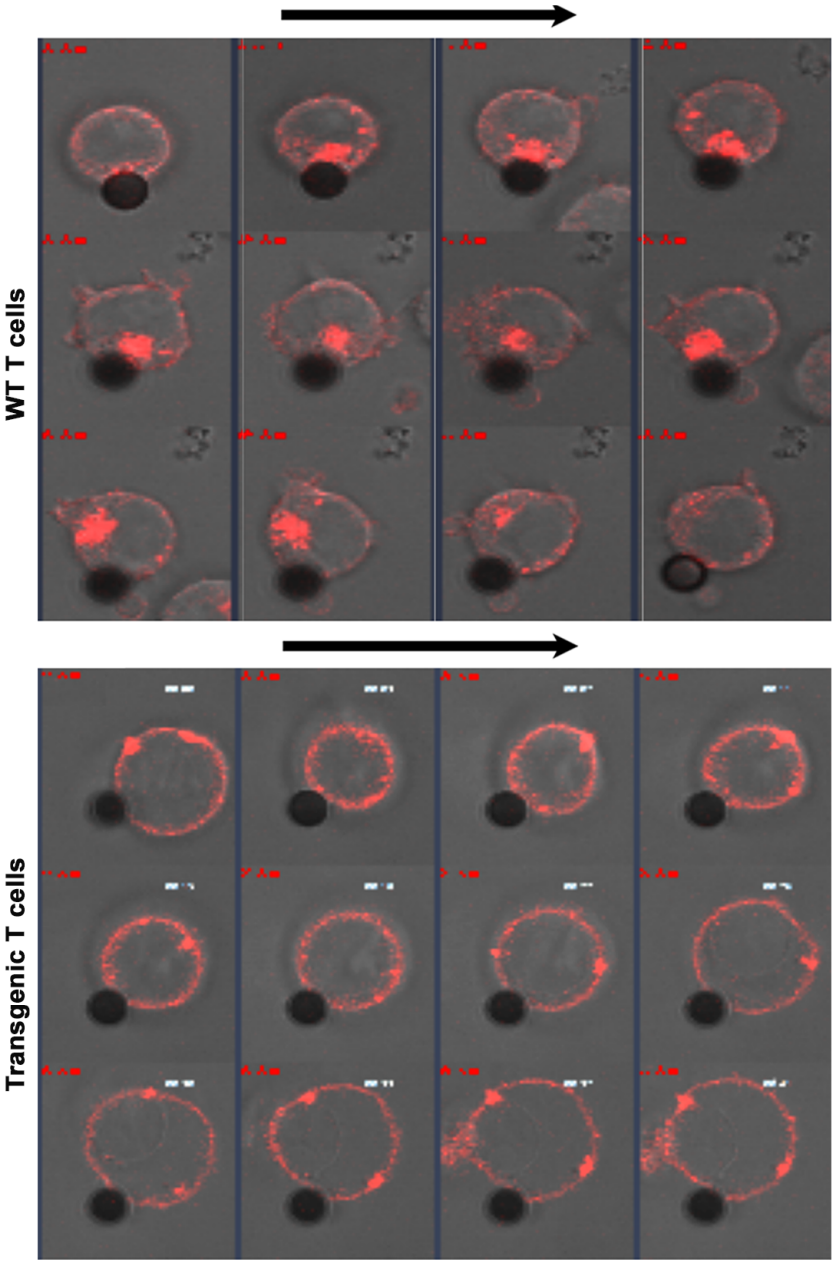
WT T cells
Transgenic T cells

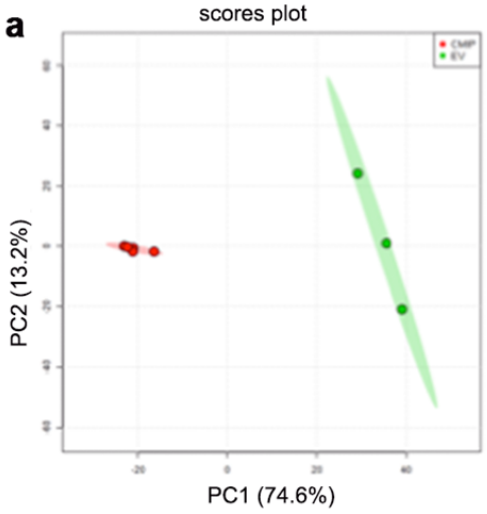

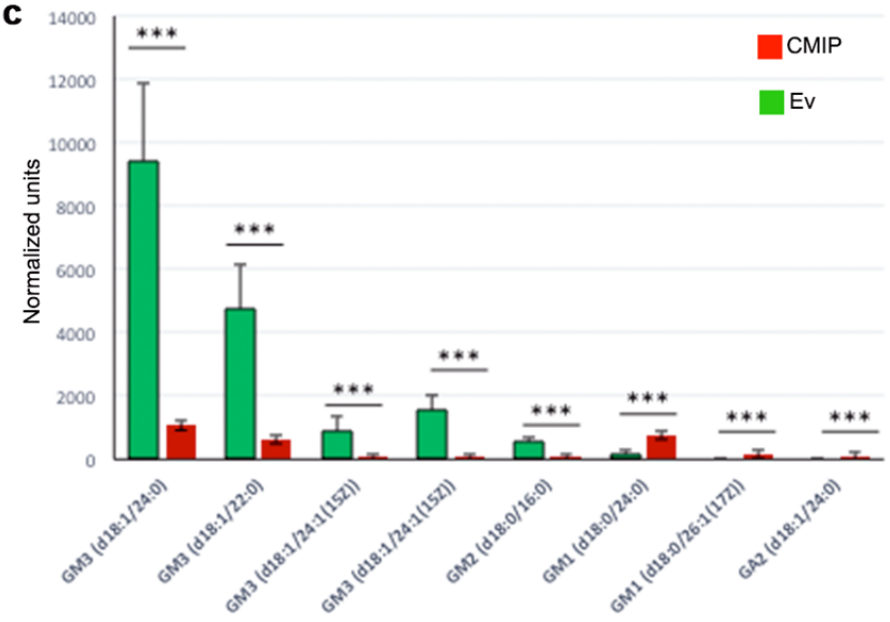

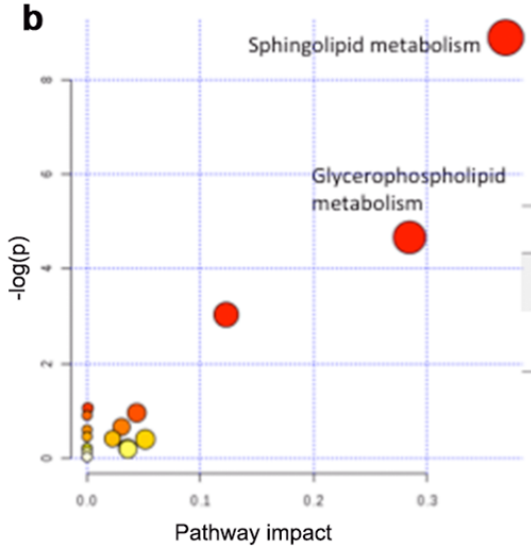

	Total	Expected	Hits	Raw p	-log(p)	Holm adjust	FDR	Impact
Sphingolipid metabolism	25	0.85168	6	0.000137	8.8944	0.010972	0.010972	0.36957
Glycerophospholipid metabolism	39	1.3286	5	0.009402	4.6668	0.74278	0.37609	0.28476

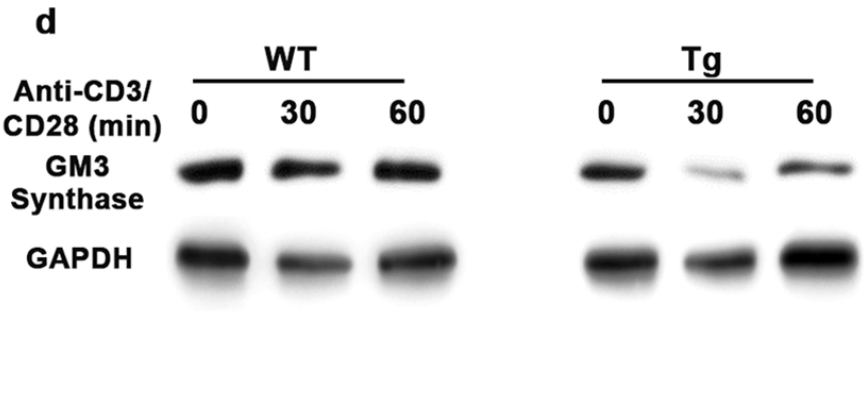

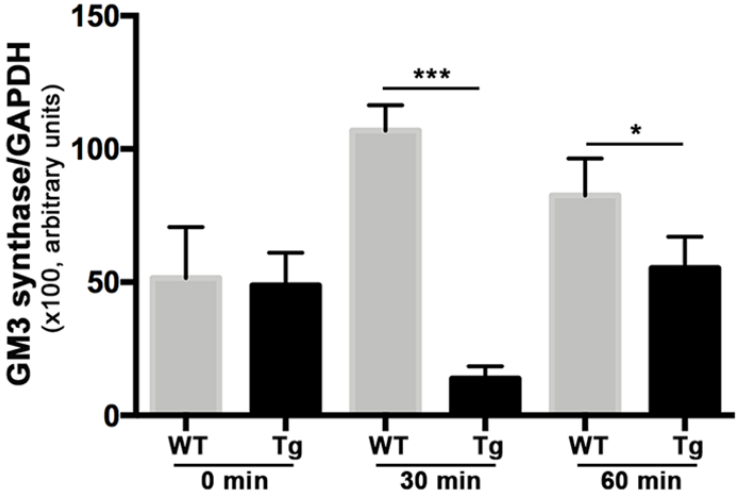

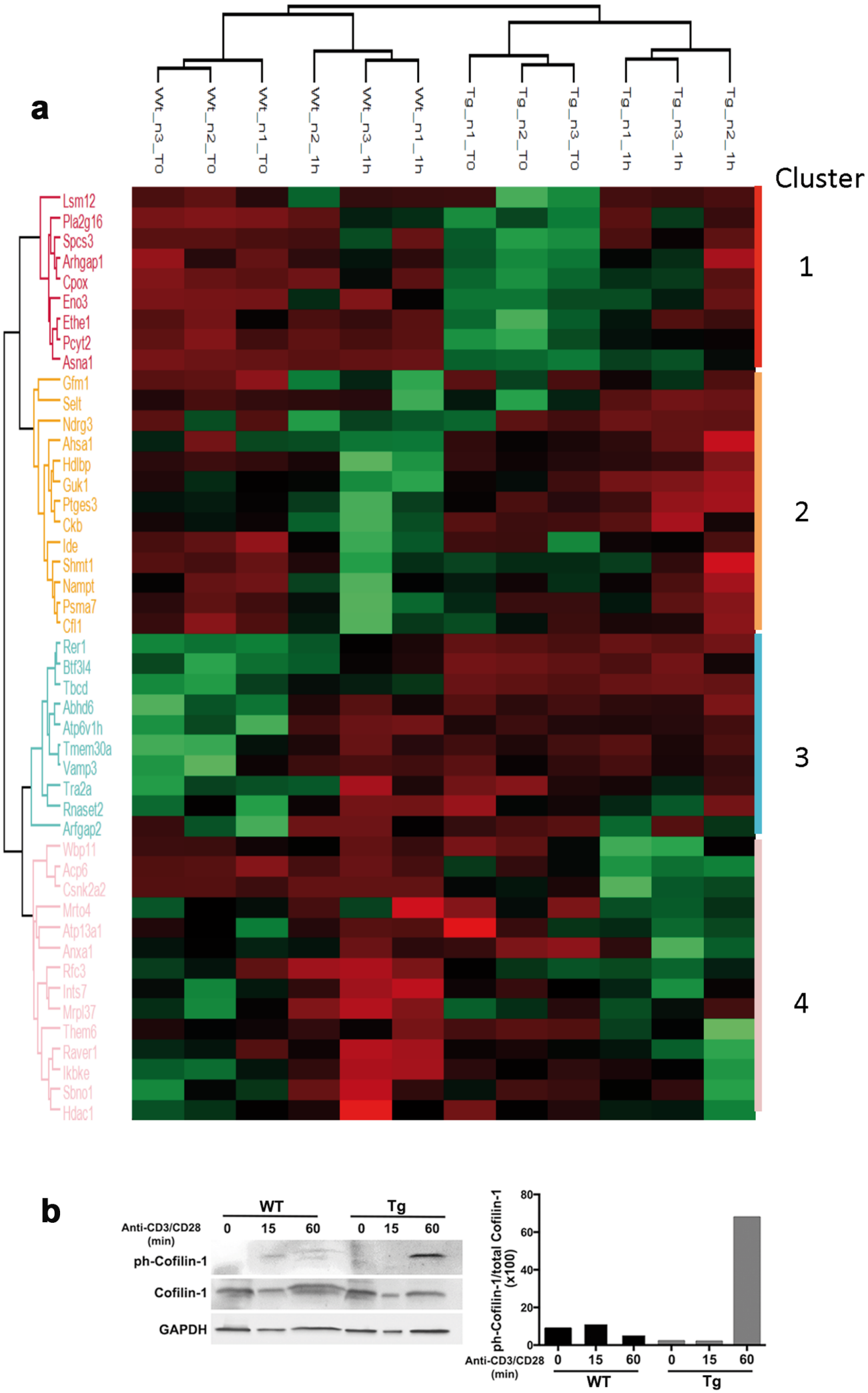
a
Wt_n3_T0
Wt_n2_T0
Wt_n1_T0
Wt_n2_1h
Wt_n3_1h
Wt_n1_1h
Tg_n1_T0
Tg_n2_T0
Tg_n3_T0
Tg_n1_1h
Tg_n3_1h
Tg_n2_1h
Cluster
Lsm12
Pla2g16
Spcs3
Arhgap1
Cpox
Eno3
Ethe1
Pcyt2
Asna1
Gfm1
Selt
Ndrg3
Ahsa1
Hdlbp
Guk1
Ptges3
Ckb
Ide
Shmt1
Nampt
Psma7
Cfl1
Rer1
Btf3l4
Tbcd
Abhd6
Atp6v1h
Tmem30a
Vamp3
Tra2a
Rnaset2
Arfgap2
Wbp11
Acp6
Csnk2a2
Mrto4
Atp13a1
Anxa1
Rfc3
Ints7
Mrpl37
Them6
Raver1
Ikbke
Sbno1
Hdac1
1
2
3
4
b
WT
Tg
Anti-CD3/CD28 (min)
0
15
60
0
15
60
ph-Cofilin-1
Cofilin-1
GAPDH
ph-Cofilin-1/total Cofilin-1 (x100)
80
60
40
20
0
Anti-CD3/CD28 (min)
0
15
60
0
15
60
WT
Tg

Table 1: Protein clusters differentially expressed between Transgenic and wild-type T-cells (see text for details)

Cluster	Two-way ANOVA p value Interaction	Protein names	Gene names
	0,0173924	ATPase Asna1	Asna1
	0,0346941	Beta-enolase	Eno3
	0,0382656	Oxygen-dependent coproporphyrinogen-III oxidase, mitochond	Cpox
	0,0198362	Rho GTPase-activating protein 1	Arhgap1
	0,00452375	HRAS-like suppressor 3	Pla2g16
	0,00564185	Ethanolamine-phosphate cytidylyltransferase	Pcyt2
	0,0447962	Protein LSM12 homolog	Lsm12
	0,00512036	Signal peptidase complex subunit 3	Spcs3
	0,0185284	Persulfide dioxygenase ETHE1, mitochondrial	Ethe1
	0,0120071	Cofilin-1	Cfl1
	0,029132	Serine hydroxymethyltransferase, cytosolic	Shmt1
	0,0207588	Selenoprotein T	Selt
	0,0308264	Creatine kinase B-type	Ckb
	0,00710747	Guanylate kinase	Guk1
	0,0328974	Activator of 90 kDa heat shock protein ATPase homolog 1	Ahsa1
	0,0272387	Elongation factor G, mitochondrial	Gfm1
	0,0336463	Vigilin	Hdlbp
	0,0136928	Nicotinamide phosphoribosyltransferase	Nampt
	0,0350412	Insulin-degrading enzyme	Ide
	0,037093	Protein NDRG3	Ndrg3
	0,0210732	Prostaglandin E synthase 3	Ptges3
	0,0274492	Proteasome subunit alpha type-7	Psma7
	0,0342864	Histone deacetylase 1	Hdac1
	0,0202517	Casein kinase II subunit alpha	Csnk2a2
	0,0197042	Annexin A1	Anxa1
	0,0223226	Protein strawberry notch homolog 1	Sbno1
	0,00719299	Integrator complex subunit 7	Ints7
	0,0246058	Protein THEM6	Them6
	0,0237745	Lysophosphatidic acid phosphatase type 6	Acp6
	0,0187061	Replication factor C subunit 3	Rfc3
	0,0401453	39S ribosomal protein L37, mitochondrial	Mrpl37
	0,0486016	WW domain-binding protein 11	Wbp11
	0,0214666	Ribonucleoprotein PTB-binding 1	Raver1
	0,0289481	mRNA turnover protein 4 homolog	Mrto4
	0,0357342	Manganese-transporting ATPase 13A1	Atp13a1
	0,0059116	Inhibitor of nuclear factor kappa-B kinase subunit epsilon	Ikbke
	0,0410545	Vesicle-associated membrane protein 3	Vamp3
	0,0413756	Transformer-2 protein homolog alpha	Tra2a
	0,000649362	V-type proton ATPase subunit H	Atp6v1h
	0,0444177	Tubulin-specific chaperone D	Tbcd
	0,00897285	Monoacylglycerol lipase ABHD6	Abhd6
	0,0217469	Cell cycle control protein 50A	Tmem30a
	0,0403846	ADP-ribosylation factor GTPase-activating protein 2	Arfgap2
	0,0478009	Ribonuclease T2	Rnaset2
	0,0380768	Transcription factor BTF3 homolog 4	Btf3l4
	0,0360256	Protein RER1	Rer1